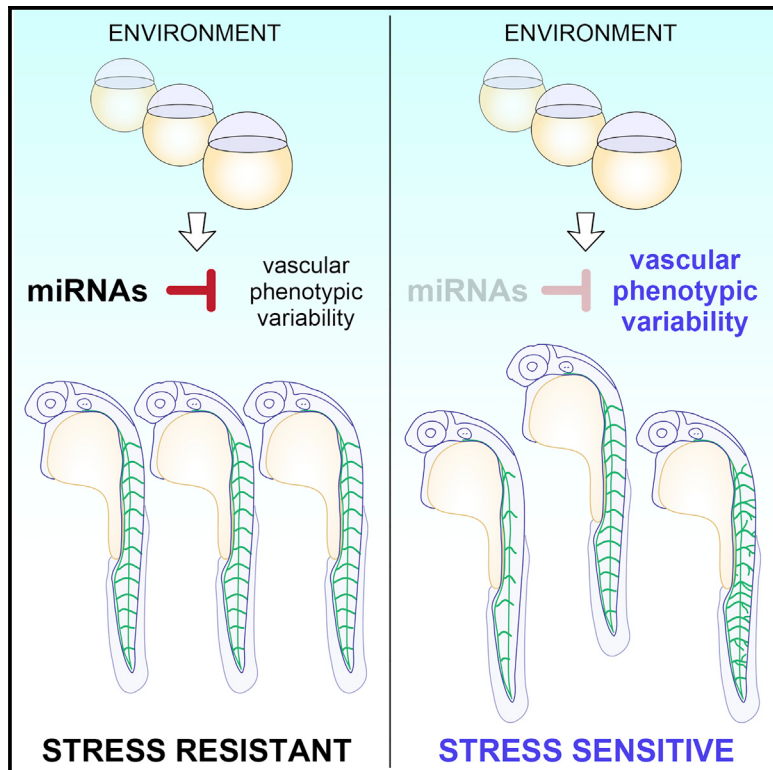


Developmental Cell

MicroRNAs Establish Uniform Traits during the Architecture of Vertebrate Embryos

Graphical Abstract



Authors

Dionna M. Kasper, Albertomaria Moro, Emma Ristori, ..., Mark Gerstein, Antonio Giraldez, Stefania Nicoli

Correspondence

stefania.nicoli@yale.edu

In Brief

Phenotypic diversity must be controlled to ensure balance between trait functionality and trait adaptability to changing environments. Kasper et al. establish that specific miRNAs limit phenotypic variation of the vascular system in a vertebrate embryo. Altered phenotypic variability resulting from miRNA loss sensitizes blood vessels to diverse environmental stresses.

Highlights

- Loss of miR-139 or miR-24 family increases the variance of developing vascular traits
- miRNA mutants with excessive trait variability are broadly sensitized to stress
- Vertebrate miRNAs provide tissue robustness to changing environments in development

MicroRNAs Establish Uniform Traits during the Architecture of Vertebrate Embryos

Dionna M. Kasper,¹ Albertomaria Moro,¹ Emma Ristori,¹ Anand Narayanan,¹ Guillermina Hill-Teran,¹ Elizabeth Fleming,³ Miguel Moreno-Mateos,³ Charles E. Vejnar,³ Jing Zhang,^{6,7} Donghoon Lee,^{6,7} Mengting Gu,^{6,7} Mark Gerstein,^{6,7,8} Antonio Giraldez,^{3,4,5} and Stefania Nicoli^{1,2,9,*}

¹Section of Cardiology, Department of Internal Medicine, Yale Cardiovascular Research Center, Yale University School of Medicine, New Haven, CT 06511, USA

²Department of Pharmacology

³Department of Genetics

⁴Yale Stem Cell Center

⁵Yale Cancer Center

Yale University School of Medicine, New Haven, CT 06510, USA

⁶Program in Computational Biology and Bioinformatics

⁷Department of Molecular Biophysics and Biochemistry

⁸Department of Computer Science

Yale University, New Haven, CT 06520, USA

⁹Lead Contact

*Correspondence: stefania.nicoli@yale.edu

<http://dx.doi.org/10.1016/j.devc.2017.02.021>

SUMMARY

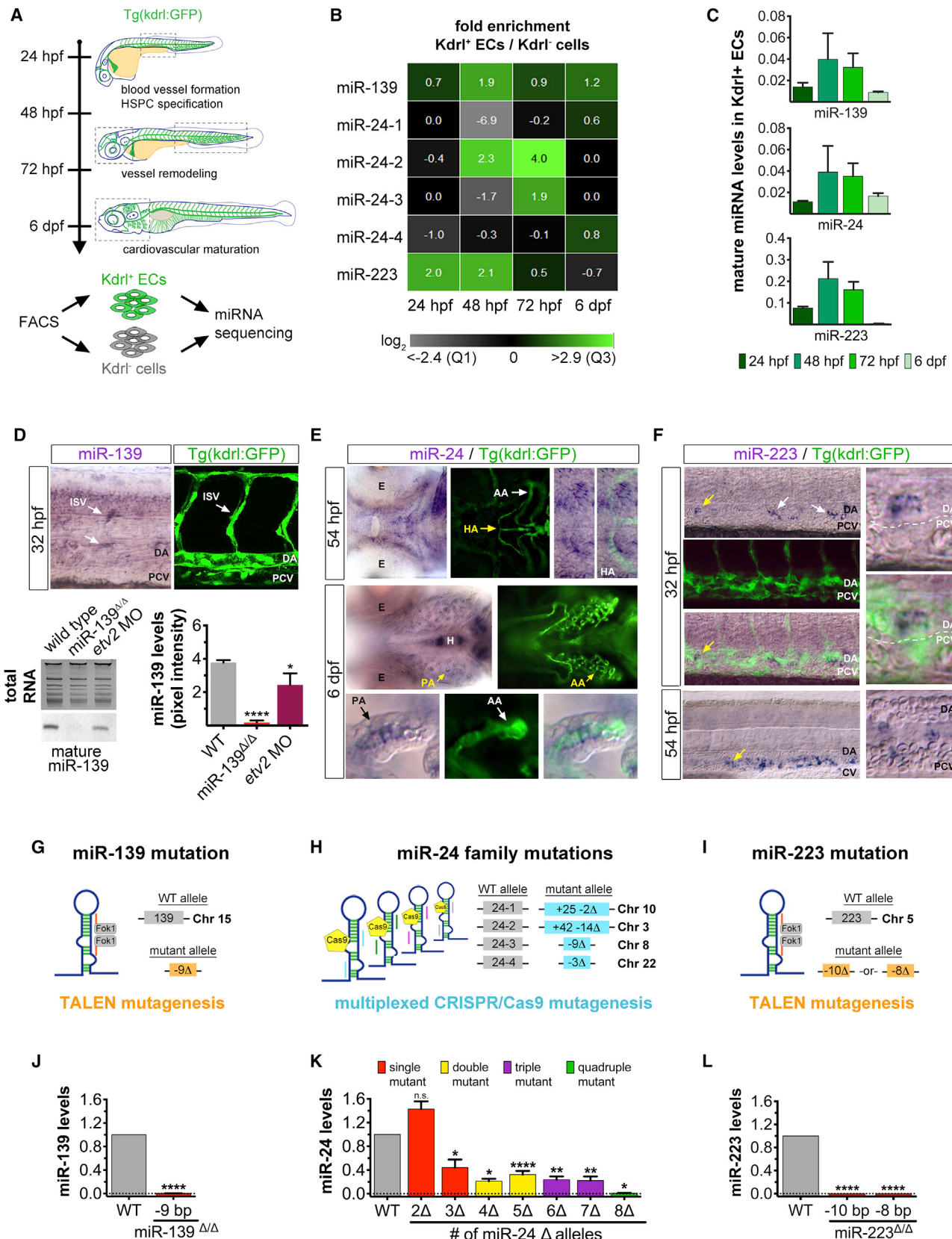
Proper functioning of an organism requires cells and tissues to behave in uniform, well-organized ways. How this optimum of phenotypes is achieved during the development of vertebrates is unclear. Here, we carried out a multi-faceted and single-cell resolution screen of zebrafish embryonic blood vessels upon mutagenesis of single and multi-gene microRNA (miRNA) families. We found that embryos lacking particular miRNA-dependent signaling pathways develop a vascular trait similar to wild-type, but with a profound increase in phenotypic heterogeneity. Aberrant trait variance in miRNA mutant embryos uniquely sensitizes their vascular system to environmental perturbations. We discovered a previously unrecognized role for specific vertebrate miRNAs to protect tissue development against phenotypic variability. This discovery marks an important advance in our comprehension of how miRNAs function in the development of higher organisms.

INTRODUCTION

Phenotypic variability is pervasive throughout biological systems, ranging from cellular attributes and tissue organization to individuals in a population (Vogt, 2015). Previous studies support the notion that phenotypic heterogeneity is established as early as embryonic development (Irmler et al., 2004; Vogt, 2015; Waddington, 1957). In invertebrates, the regulation of variance in developing traits provides cells or organisms with adaptive responses to dynamic environments (Ambros et al., 2003; Cassidy et al., 2013; Frankel et al., 2010; Rutherford and Lindquist, 1998; Vogt, 2015). Unfortunately, how vertebrates regulate phenotypic

heterogeneity during development remains incompletely understood. In humans, the study of phenotypic heterogeneity has been predominantly concerned with disease traits. For example, in cancer and cardiovascular disorders, a single population with a common genetic insult can manifest a diverse spectrum of disease phenotypes that is highly dependent on environmental risk factors (Liu et al., 2014; Marusyk et al., 2012; Queitsch et al., 2012; Weiss et al., 2012). Deciphering mechanisms regulating trait variance in vertebrate developmental models could reveal how an individual's phenotype responds to changing physiological or pathological conditions.

Phenotypic heterogeneity is primarily generated by fluctuations in gene expression that stem from genetic, environmental, and stochastic variation (Raj and van Oudenaarden, 2008). MicroRNA (miRNA) regulation confers genetic robustness to gene networks and therefore has been recognized as one of the most effective mechanisms to limit gene expression inaccuracies (Blevins et al., 2015; Burke et al., 2015; Cassidy et al., 2013; Ebert and Sharp, 2012; Herranz and Cohen, 2010; Schmiedel et al., 2015; Yatsenko and Shcherbata, 2014). miRNAs tune or buffer protein output by targeting mRNAs for translational inhibition or decay (Bartel, 2009). The majority of protein-coding genes are controlled by miRNAs, and a single miRNA can rapidly repress hundreds of transcripts (Baek et al., 2008; Selbach et al., 2008). miRNAs can collectively regulate positive and negative effectors of a genetic pathway and function in regulatory feedback loops, thereby providing precision to signaling cascades (Ebert and Sharp, 2012; Herranz and Cohen, 2010; Verma and Cohen, 2015). Based on these powerful functions of miRNAs as genetic buffers, loss of miRNA activity should influence trait variance as a default phenotype. In support of this hypothesis, altered phenotypic variability of developing traits was found in a handful of fly and worm miRNA mutants (Cassidy et al., 2013, 2016; Kugler et al., 2013; Ren and Ambros, 2015). Surprisingly, however, this has remained untested in vertebrates. miRNA mutant studies have not directly examined phenotypic heterogeneity, as they measured trait averages (means) alone



(legend on next page)

and disregarded the distribution (variance) of the phenotype (Felix and Barkoulas, 2015; Park et al., 2010, 2012; Vidigal and Ventura, 2015). Thus, the analysis of phenotypic heterogeneity and its functional consequences have never been described in these miRNA knockouts.

Here, we used the zebrafish cardiovascular system as a platform to probe the establishment of trait means and variance in the absence of miRNA activity. We analyzed the phenotypes associated with the loss of three endothelial-expressed miRNAs and their respective vascular target genes. We discovered that while vascular traits lacking specific miRNAs developed with a mild to no change in mean, they were characterized by an unexpected increase in variability. Remarkably, only miRNA mutants with altered vascular phenotypic heterogeneity were sensitized to a broad range of chemical and environmental perturbations. Our results establish that distinct miRNAs stabilize phenotypic variability of developing vertebrate traits as a way to provide tissue robustness to changing environments.

RESULTS

Identification and Mutagenesis of Endothelial miRNAs

We used the zebrafish embryonic cardiovascular system to investigate a function for miRNAs in standardizing phenotypic expression. Cardiovascular phenotypes are easily detectable and measured in this model because of the external growth and optical transparency of the embryo. These traits include the angiogenic sprouting of endothelial cells to form blood vessels beginning at ~24 hr post fertilization (hpf), hemogenic endothelium specification of hematopoietic stem/progenitor cells (HSPCs) starting at ~32 hpf, and vessel remodeling and maturation from 48 hpf to 6 days post fertilization (dpf) (Figure 1A) (Bertrand et al., 2010; Isogai et al., 2001, 2003).

Using this well-established platform, we first performed Illumina sequencing of miRNAs from endothelial (*Kdrl:GFP⁺*) and non-endothelial (*Kdrl:GFP⁻*) cells in 24 hpf to 6 dpf embryos expressing the vascular-specific transgene *Tg(kdrl:gfp)^{la116}* (Figure 1A). We found 46 miRNAs highly expressed and/or enriched in endothelial cells in at least one developmental stage, which we term “endothelial miRNAs” (Figures 1B, 1C, and S1A).

To thoroughly assess the requirement of miRNAs in regulating phenotypic heterogeneity, we examined their function in three diverse vascular contexts. Specifically, we characterized the miR-139 and miR-223 single miRNA genes, and the miR-24 family, which comprises four genes that are processed into the same mature miRNA (Figure S1B). These miRNAs showed differential expression during vascular development as well as localization to unique vascular beds (Figures 1B–1F). Specifically, we detected miR-139 expression and activity in the intersegmental vessels (ISVs) of the trunk vasculature at 32 hpf (Figures 1D and S1C–S1E). miR-24 expression at 54 hpf was limited to the ventral craniofacial region within pharyngeal arches, endoderm, and mesenchyme including aortic arch endothelium. By 6 dpf, miR-24 became solely restricted to vascular cells (Figure 1E). miR-223 was observed at 32 hpf in hemogenic endothelium along the ventral wall of the dorsal aorta (DA) where HSPCs are specified, and at subsequent sites of blood production at 54 hpf and 6 dpf (Figures 1F and S1F).

Next, we generated loss-of-function alleles to analyze the roles of miR-139, miR-24 family, and miR-223. To form the functional ~22-bp miRNA, the miRNA precursor transcript must be folded into a precise hairpin structure for Drosha/DGCR8 and Dicer cleavage (Ha and Kim, 2014). Therefore, we employed genome-editing techniques to induce mutations (referred to in the text as Δ) that interfere with miRNA processing as a way to disrupt miRNA activity (Figures 1G–1I and S2A). TAL effector

Figure 1. Generation of Endothelial miRNA Mutants in Zebrafish

(A) Experimental procedure to identify miRNAs expressed in fluorescence-activated cell (FAC)-sorted *Kdrl:GFP⁺* endothelial cells and *Kdrl:GFP⁻* non-endothelial cells during the four major stages of zebrafish vascular development. Dashed boxes outline the regions examined for cardiovascular phenotypes in endothelial miRNA mutant embryos (see Figure S2C).

(B) Heatmap depicts miRNA reads per million in *Kdrl:GFP⁺* endothelial relative to non-endothelial cells for two biological replicates. Color scale ranges from the first quartile (Q1) to the third quartile (Q3) fold-enrichment values for all 46 endothelial miRNAs identified (see Figure S1A).

(C) Average mature miRNA levels relative to U6 small nuclear RNA (snRNA) expression as determined by qRT-PCR in FAC-sorted *Kdrl:GFP⁺* endothelial cells at the indicated developmental stages.

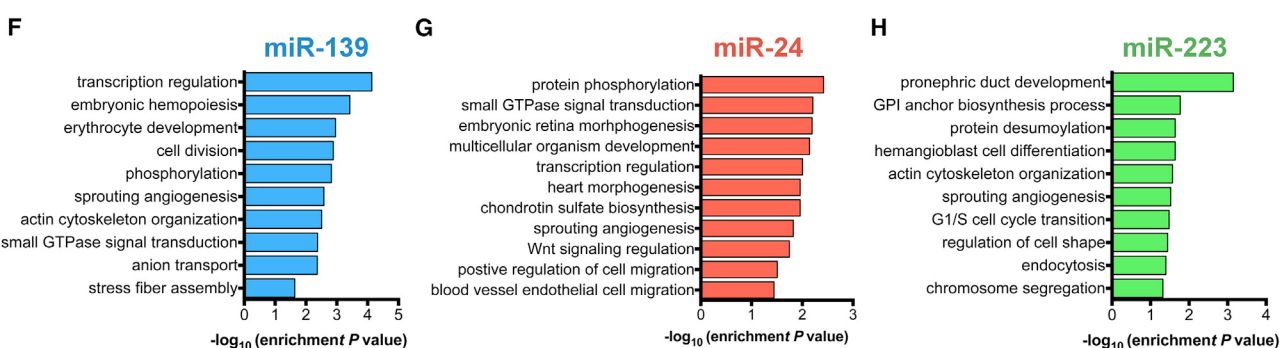
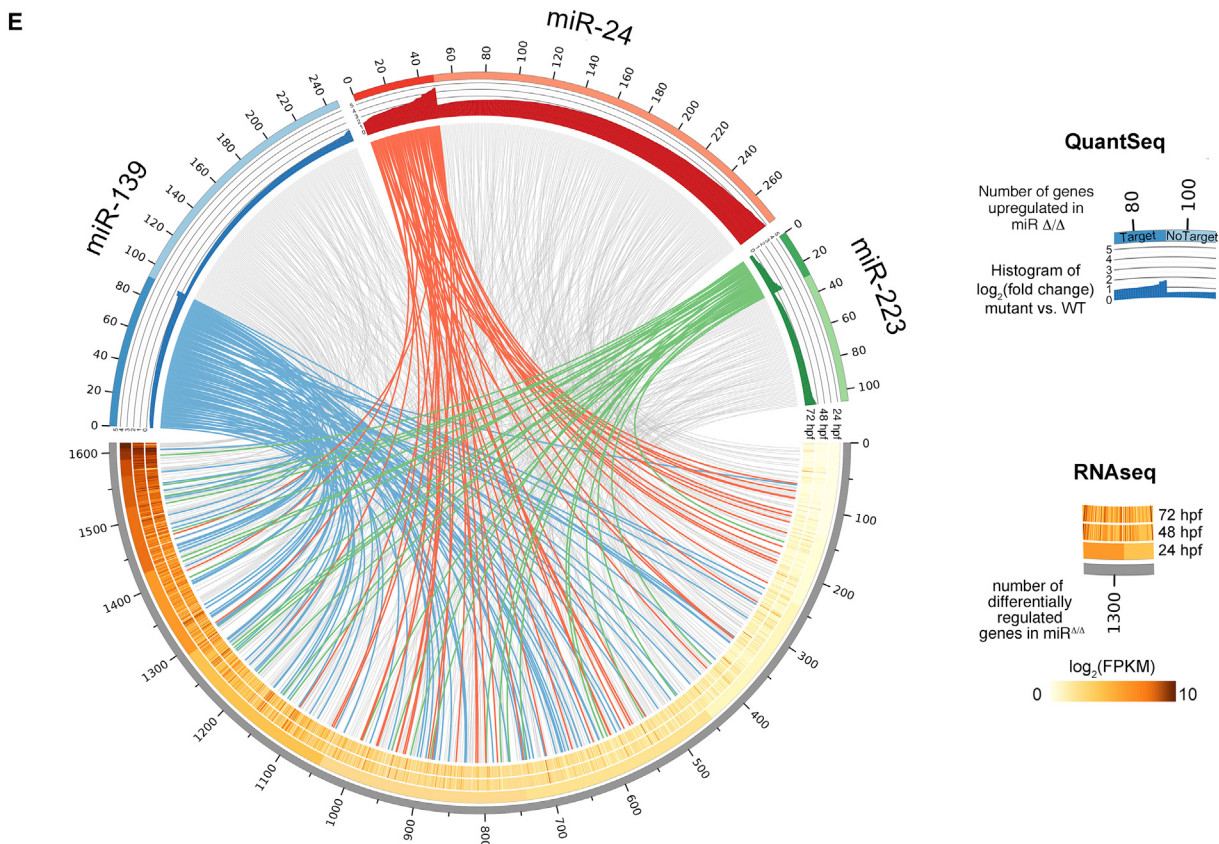
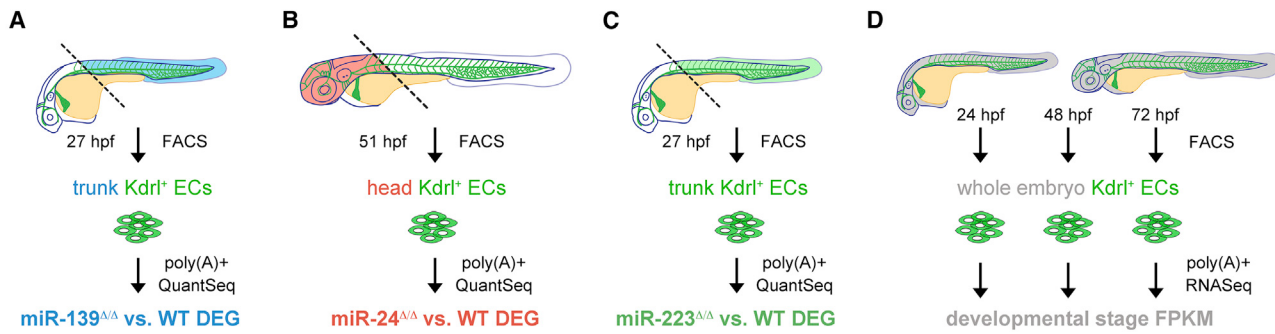
(D) Top: Lateral trunk view (20×) of wild-type embryos showing whole-mount *in situ* hybridization (WISH) for mature miR-139, labeling cells within the ISV position. Confocal image (25×) shows the relative position of ISVs in the lateral trunk. Bottom: northern blot and respective quantification showing mature miR-139 expression relative to total RNA in three biological replicates of 32-hpf embryos treated as indicated. Consistent with miR-139 expression in ISVs, mature miR-139 levels were diminished in *etv2* morphant embryos, which lack these trunk vessels (Pham et al., 2007).

(E) Mature miR-24 localization in the ventral head of wild-type embryos in relation to *Kdrl:GFP⁺* vasculature at the indicated developmental stages (20×). By 6 dpf, miR-24 remained in vascular cells but was excluded from cartilaginous and bone structures. Arrows point to anatomic landmarks. Yellow arrows point to the region captured in zoomed-in images (40×).

(F) Mature miR-223 localization in the lateral *Kdrl:GFP⁺* trunk vasculature of wild-type embryos at the indicated stages (20×). At 54 hpf, miR-223 is expressed in cells within the caudal hematopoietic tissue located between the DA and CV. Arrows show examples of miR-223⁺ cells. Yellow arrows point to the region captured in magnified images.

(G–I) Schematic representation of the genome-editing strategies employed to mutagenize endothelial miRNAs. TALENs and a multiplexed CRISPR/Cas9 system were targeted to miRNA precursor genomic sequences to prevent mature miRNA formation. Gray boxes represent the wild-type allele. Colored boxes reveal the nature of the mutant allele. See also Figure S2A.

(J–L) qRT-PCR showing average mature miRNA expression normalized to U6 snRNA levels in miRNA mutant embryos (J), embryo heads (K), or adult fins (L) relative to wild-type. For miR-24 mutants, genotypes were categorized as a single mutant when two ($\Delta 2$, miR-24-1Δ/Δ) and three ($\Delta 3$, e.g., miR-24-1^{+/+}/Δ 4Δ/Δ) miR-24 alleles were mutated, up to a quadruple mutant that lacked all eight miR-24 alleles ($\Delta 8$, miR-24-1Δ/Δ 2Δ/Δ 3Δ/Δ 4Δ/Δ). See also Figure S2B. Bar plots represent mean ± SEM and significance calculations are relative to wild-type embryos. n.s., not significant ($p > 0.05$); * $p \leq 0.05$, ** $p \leq 0.01$, *** $p \leq 0.0001$, two-tailed Student's t test. qRT-PCR data represent two to five biological replicates. Ten to 20 embryos from at least two different clutches were examined by WISH. AA, aortic arches; DA, dorsal aorta; CV, caudal vein; E, eye; EC, endothelial cell; H, heart; HA, hypobranchial artery; ISV, intersegmental vessel; PA, pharyngeal arch; PCV, posterior cardinal vein.



(legend on next page)

nucleases (TALENs) produced a 9Δ bp deletion in the miR-139 gene and 10Δ bp and 8Δ bp deletion alleles in the miR-223 locus (**Figures 1G** and **1I**). In addition, injection of multiplexed pairs of CRISPR guide RNAs with Cas9 mRNA resulted in the concurrent mutagenesis of the four miR-24 family genes (**Figure 1H**). We analyzed mature miRNA levels in mutants homozygous for miR-139 (miR-139Δ/Δ) and miR-223 (miR-223Δ/Δ), and in an miR-24 mutant allelic series (**Figures 1J–1L** and **S2B**). Mature miRNA expression was completely absent in miR-139Δ/Δ and miR-223Δ/Δ, and was progressively diminished and ultimately lost from miR-24 single to quadruple mutants (**Figures 1J–1L**). Thus, our generated alleles enabled loss of miRNA function studies.

Genome-wide Analysis of miR-139, miR-24, and miR-223 Regulated Vascular Target Genes

miR-139Δ/Δ, miR-24 mutant allelic series, and miR-223Δ/Δ zebrafish lacked gross morphological defects, and grew to fertile adults (data not shown). Therefore, we investigated the fine vascular phenotypes controlled by these miRNAs by identifying endothelial transcripts dependent on the activity of each miRNA. As mRNA destabilization is a common mechanism of miRNA repression (**Baek et al., 2008**), we carried out comparative mRNA transcriptome profiling between miRNA mutant and wild-type endothelial cells isolated from the anatomical regions corresponding to the expression of each miRNA (**Figures 1D–1F** and **2A–2C**). Endothelial cells were collected from 27-hpf dissected trunk tissue of miR-139Δ/Δ and miR-223Δ/Δ embryos and from 51-hpf head tissue of miR-24 double, triple, and quadruple mutant mixed-genotype clutch, which all displayed a significant loss of miRNA expression (**Figures 1J–1L** and **2A–2C**). Additionally we deep-sequenced endothelial mRNAs isolated from 24- to 72-hpf whole embryos for comparison to these regional profiles (**Figure 2D**).

We used the Circos software package to better visualize the regulatory activity of each miRNA. Links represent individual genes stabilized in miRNA-deficient endothelial cells and point to their vascular expression between stages (**Figure 2E**). Approximately 18%–37% of the upregulated transcripts in each dataset contained at least one miRNA-binding motif within their 3' UTR (colored links), which corresponded to 1%–2% of all predicted target genes expressed in endothelial cells (**Figure 2E** and data not shown). Therefore, only a subset of vascular target genes depended on miR-139, miR-24, or miR-223 activity at these developmental stages.

Examination of gene ontology (GO) terms for the identified target genes revealed several terms related to vascular growth

and hematopoiesis (**Figures 2F–2H**). GO terms significantly enriched among miR-139 target genes included erythrocyte development, sprouting angiogenesis, and other cell migration processes such as small guanosine triphosphatase signal transduction and cytoskeleton organization (**Wakayama et al., 2015**) (**Figure 2F**). Analysis of miR-24 target genes revealed similar cell motility terms including sprouting angiogenesis and vascular cell migration, as well as contained chondroitin sulfate biosynthesis involved in cartilage production (**Holmboe et al., 2012**) (**Figure 2G**). In comparison, miR-223 target gene categories were often related to stem cell function such as hemangioblast cell differentiation, G₁/S cell-cycle transition, and cell-shape regulation (**Gritz and Hirschi, 2016**) (**Figure 2H**).

Taken together, we identified specialized endothelial gene networks dependent on miR-139, miR-24, and miR-223 function. Consistent with their diverse vascular expression patterns, miR-139 and miR-24 targets converged on traits involved in vascular growth and morphogenesis, whereas miR-223 targets centered on HSPC specification-related processes.

Loss of miR-139 Increases Variability in Endothelial Cell Filopodia Number

We searched for molecular phenotypes occurring in vascular development and hematopoiesis in miR-139Δ/Δ due to the enrichment of these biological processes in miR-139-regulated target genes (**Figures 2F** and **S2C**). While most angiogenic markers, vessel growth, and blood production were unaffected (**Figures 3A**, **3B**, and **S3A–S3C**), we found altered chemokine receptor *cxcr4a* expression in miR-139Δ/Δ ISVs at 32 hpf (**Figures S3D** and **S3E**). Filopodia membrane extensions have been associated with chemokine-regulated cell migration and are numerous on endothelial cells during ISV formation (**Isogai et al., 2003; Meyen et al., 2015**). As miR-139 was detected in ISVs (**Figures 1D** and **S1C–S1E**), we assessed filopodia on single endothelial cells in these vessels.

At 32 hpf, the average number of ISV filopodia was increased on cells lacking miR-139 activity (**Figures 3C** and **3D**). Strikingly, we also detected a greater variability of these cytoplasmic projections in miR-139Δ/Δ compared with wild-type embryos. While wild-type endothelial cells possessed a specific distribution of filopodia number, miR-139Δ/Δ cells exceeded this range either by completely lacking or having a multitude of filopodia (**Figures 3C**, **3E**, and **3F**). Quantification of this heterogeneous phenotype revealed a change in distribution density, which was confirmed as significant by Levene's test (**Felix and Barkoulas, 2015; Schultz, 1985**) (**Figure 3E**). In agreement, the SD of this trait is

Figure 2. Genome-wide Identification of Vascular Target Gene Networks Regulated by Endothelial miRNAs

(A–D) Strategy to identify vascular transcripts regulated by endothelial miRNAs. Kdrl:GFP⁺ endothelial cells were FACS-sorted from dissected 27-hpf wild-type, miR-139Δ/Δ, and miR-223Δ/Δ trunk tissue (A and C) or 51-hpf wild-type and miR-24Δ/Δ head tissue (B), and used to generate QuantSeq 3' mRNA libraries to identify differentially expressed genes (DEG) between wild-type and mutant samples. miR-24Δ/Δ samples represent a mixed clutch of double, triple, and quadruple mutant genotypes. Standard mRNA-sequencing libraries were generated to assess endothelial cell gene expression levels in whole embryos across the indicated developmental times (D).

(E) Circos plot depicting the dynamic regulation of vascular genes upregulated (\log_2 -fold change [FC] ≥ 0.26 , $p \leq 0.05$) in miR-139Δ/Δ trunk (blue sector), miR-24Δ/Δ head (red sector), and miR-223Δ/Δ trunk (green sector) endothelial cells compared with wild-type controls. Colored and gray links indicate upregulated vascular genes that contain or lack a computationally predicted target site for the indicated miRNA, respectively. Links connect to stage-specific heatmaps in the gray sector, which show overall expression levels of genes differentially expressed between wild-type and mutant Kdrl:GFP⁺ endothelial cells in terms of FPKM (fragments per kilobase of exon per million mapped reads).

(F–H) Bar plots of the most significantly enriched gene ontology (GO) terms among upregulated (\log_2 -FC ≥ 0.26) vascular target genes for each miRNA. GO terms have $-\log_{10}$ (enrichment $p < 0.05$).

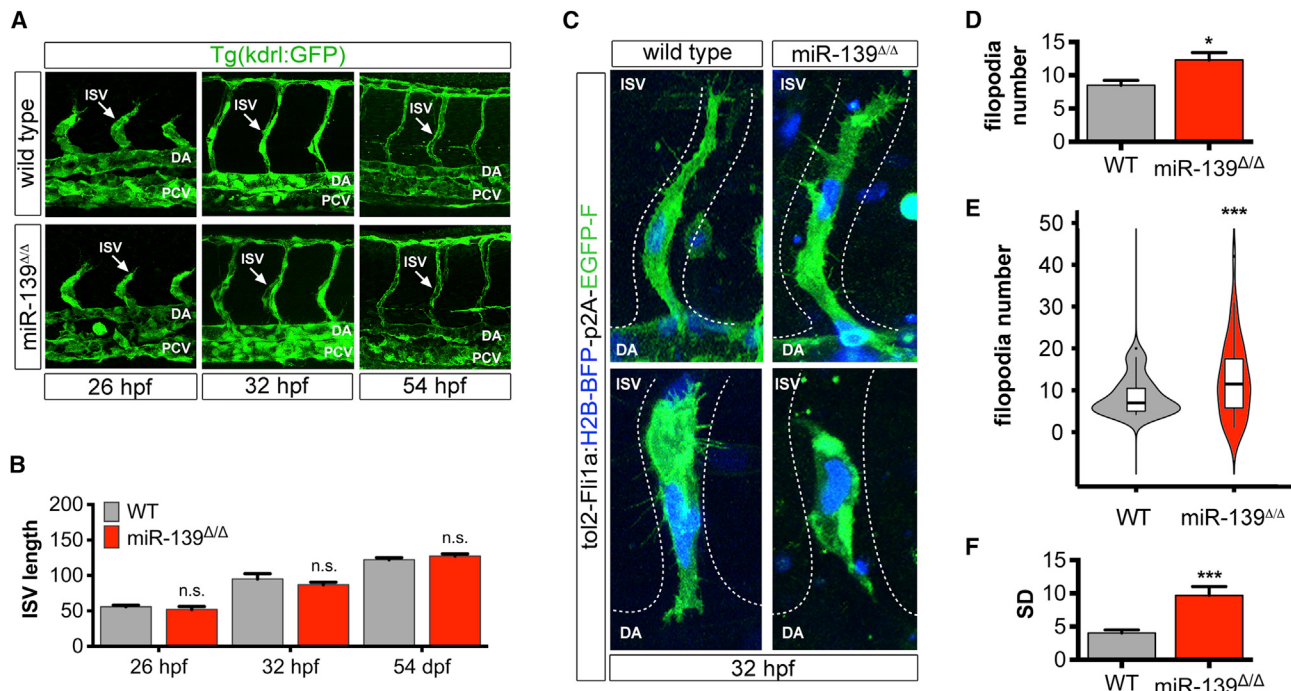


Figure 3. miR-139 Homozygous Mutants Exhibit Heterogeneity in Endothelial Cell Filopodia Number

(A) Lateral view (25×) of *Kdrl:GFP*⁺ trunk vasculature at the indicated developmental stages. Arrows point to ISVs.

(B) Average ISV length (μm) was determined from confocal projections (n = 9–18). Bar plots show mean ± SEM.

(C) Representative images (40×) of single endothelial cells expressing *tol2-Fli1a-H2B-BFP-p2A-EGFP-farnesyl* vector in wild-type and miR-139^{Δ/Δ} ISVs. miR-139^{Δ/Δ} images depict endothelial cells with excessive (top) or few (bottom) filopodia. Endothelial cell nuclei are in blue and membranes are in green.

(D) Bar plots show the average of replicate means ± SEM of endothelial cell filopodia number (n = 9 replicates).

(E) Violin plots show filopodia number probability density distributions. Solid lines in box plots depict median values. Phenotypic variability was significantly different from wild-type, ***p = 9.46 × 10⁻⁴ by Levene's test (n = 36 cells).

(F) Bar plots show average replicate SD ± SEM of endothelial cell filopodia number (n = 9 replicates).

Significance calculations were relative to wild-type embryos. n.s., not significant (p > 0.05); *p ≤ 0.05, ***p ≤ 0.001, two-tailed Mann-Whitney U test unless otherwise indicated. Abbreviations as defined in Figure 1. See also Figure S3.

significantly increased in mutant endothelial cells (Figure 3F). Thus, the more diverse spectrum of endothelial cell filopodia number in miR-139^{Δ/Δ} embryos indeed resulted from a change in phenotypic variability.

In summary, miR-139^{Δ/Δ} exhibit ISV morphology similar to that of wild-type, but possess endothelial cells that display a broader range of filopodia number. In this fashion, miR-139 is required to standardize ISV endothelial cell phenotypes.

Progressive miR-24 Depletion Enhances Phenotypic Variability in Hypobranchial Artery Morphogenesis

Intrigued by the marked increased variability of endothelial cell morphology in miR-139^{Δ/Δ} embryos, we examined the miR-24 mutant allelic series to investigate whether miRNAs could influence phenotypic heterogeneity in a second vascular developmental context. Analysis of this vast collection of mutant genotypes also allowed us to explore how phenotypic heterogeneity responds to a stepwise loss of miRNA gene copies (Figure 1K).

We screened miR-24 mutants with craniofacial morphology and vascular markers, since miR-24 expression and activity were related to both pharyngeal and aortic arch development (Figures 1E and 2G). Patterns of *sox9a*⁺ chondrocyte progenitors

and derived cartilaginous structures formed properly in miR-24^{Δ/Δ} embryos, and thus ruled out a substantial contribution of this miRNA to craniofacial skeletal formation (Figure 4A). Confocal analysis of the developing ventral head vasculature did unveil a requirement for miR-24 in the morphogenesis of the hypobranchial artery (HA), which together with the aortic arches supplies blood to ventral craniofacial tissues (Isogai et al., 2001). Embryos lacking at least three miR-24 copies exhibited partial HA sprouting at 54 hpf, and by 6 dpf had a hypoplastic HA and less complex aortic arches, which correlated well with diminishing mature miR-24 levels in these vessels (Figures 4B and S4A). Patterning of other cranial vessels was comparable between all miR-24^{Δ/Δ} genotypes and wild-type embryos (Figure S4B).

While mean HA size was significantly smaller only in miR-24 triple and quadruple mutants, we found a marked increase in phenotypic heterogeneity prior to the appearance of the sprouting defect (Figures 4B–4E). Progressive depletion and loss of miR-24 expression resulted in embryos with a continuum of phenotypes ranging from a properly formed to absent HA (Figure 4B). Remarkably, miR-24 single and double mutant embryos had significantly different HA length variance despite possessing an HA of normal size on average (Figures 4C–4E). Therefore, the

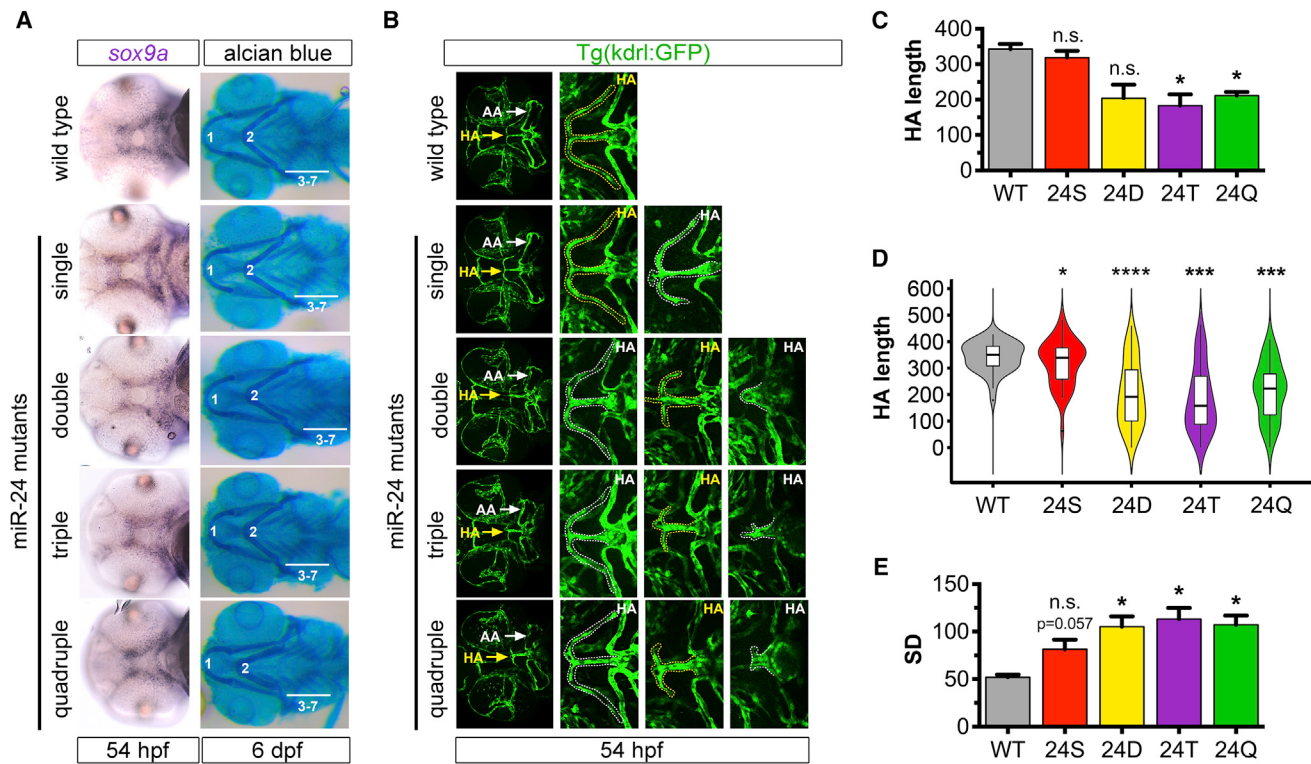


Figure 4. Enhanced Phenotypic Variability in Hypobranchial Artery Sprouting with Diminishing miR-24 Activity

(A) sox9a WISH labeling chondrocyte progenitors (left) and Alcian blue-stained cartilage (right) in the ventral head of wild-type and miR-24 mutant embryos ($n \geq 6$ for all genotypes except $n = 2$ for quadruple mutants). Numbers indicate the position of pharyngeal arches 1–7. miR-24 genotypes are categorized as in Figure S2B.

(B) Ventral view (25×) of 54-hpf head vasculature. Magnified images depict the spectrum of HA phenotypes (dotted outlines) for each genotype. The HA sprout most representative of the genotype is indicated with a yellow arrow and is depicted in the zoomed-in picture with a yellow HA label. White arrows point to aortic arches (AA).

(C) Bar plots show the average of replicate means \pm SEM of HA length (μm) at 54 hpf ($n = 4$ replicates).

(D) Violin plots show 54-hpf HA length (μm) probability density distributions. Solid lines in box plots depict median values. Phenotypic variability was statistically different from wild-type as determined by the Levene's test ($n = 40$ embryos). Single: * $p = 0.04$; double: *** $p = 5.77 \times 10^{-6}$; triple: *** $p = 3.46 \times 10^{-4}$; quadruple: ** $p = 7.57 \times 10^{-4}$.

(E) Bar plots show average replicate SD \pm SEM of HA length (μm) at 54 hpf ($n = 4$ replicates).

For all bar blots, S, single; D, double; T, triple; Q, quadruple mutant. Significance calculations were relative to wild-type embryos. n.s., not significant ($p > 0.05$); * $p \leq 0.05$, ** $p \leq 0.01$, *** $p \leq 0.001$, two-tailed Mann-Whitney U test unless otherwise indicated.

miR-24 expression level resulting from the loss of one miR-24 gene copy coincided with the onset of increased HA phenotypic variability (Figure 4D).

These data show that the gradual loss of miR-24 activity resulted in a broader range of smaller HA sizes and increased the probability that these embryos have a phenotypic value outside the wild-type spectrum. Taken together, miR-24 ensures reproducible HA vascular morphogenesis.

Loss of miR-223 Affects HSPC Formation without a Change in Phenotypic Variability

Our study of miR-139 and the miR-24 family provides compelling evidence that miRNAs limit phenotypic diversity in vertebrate development. Therefore, we tested the generality of this miRNA function by investigating a third vascular context in the absence of miR-223 activity.

In accord with miR-223 expression in HSPCs and enrichment of hematopoiesis terms among miR-223-regulated targets (Fig-

ures 1F, 2H, and S5A), miR-223Δ/Δ showed enhanced *cmyb*⁺ expression resulting from a specific increase in *kdr*⁺*cmyb*⁺ cells (Figures 5A–5D and S5B). Consequently, myeloid, but not lymphoid markers were expanded in embryos lacking miR-223 (Figures S5C–S5F), similar to the blood cell phenotypes described in the adult miR-223 knockout mouse (Johnnidis et al., 2008). Most notably, we did not observe a statistical change in *kdr*⁺*cmyb*⁺ cell number variance between wild-type and miR-223Δ/Δ embryos (Figures 5E and 5F).

We conclude from these data that miR-223 regulates the average number of HSPCs without affecting the distribution of this trait. Thus, limiting the phenotypic variability of a trait is not a default function of miRNAs during development.

Phenotypic Heterogeneity in miRNA Mutants Confers Sensitization to Diverse Stressors

Mutations in miR-139 and the miR-24 family, but not miR-223, significantly affected both vascular cell trait means and

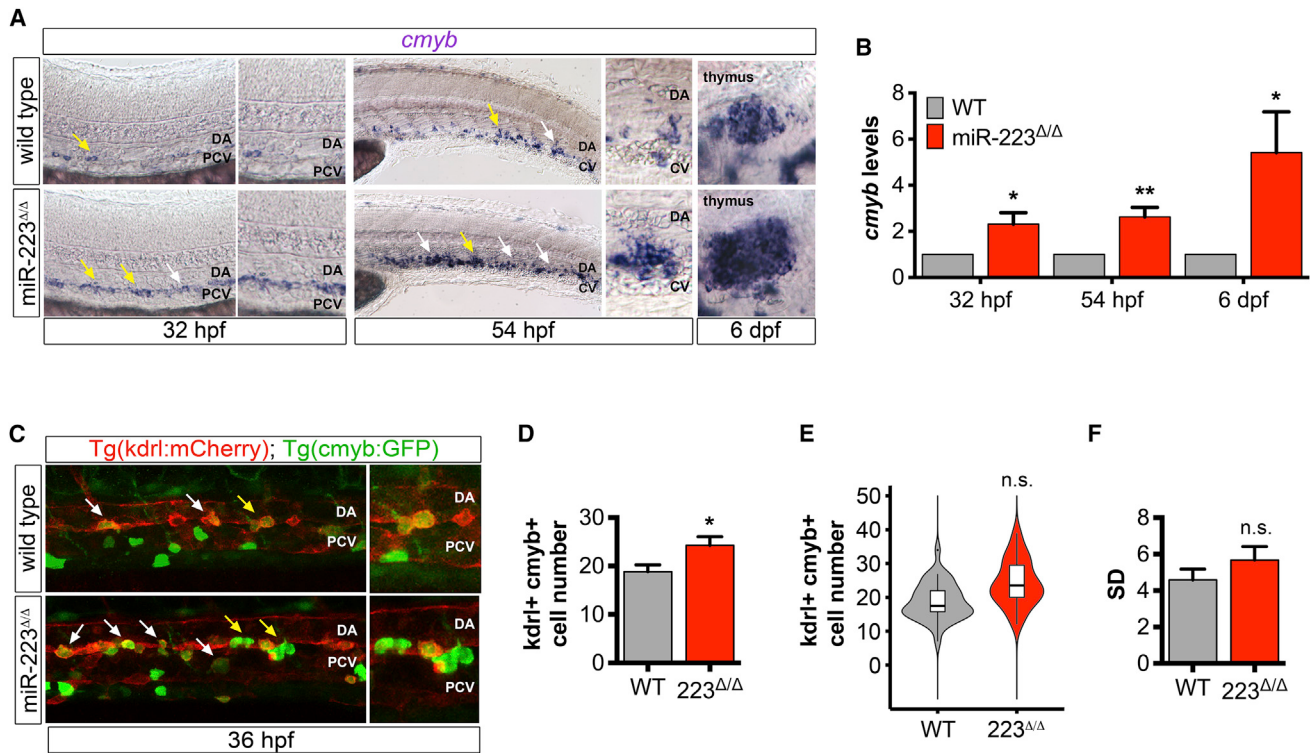


Figure 5. miR-223 Does Not Regulate Phenotypic Variability of HSPC Number

(A) WISH of HSPC marker *cmyb* at transient sites of hematopoiesis, namely the DA ventral wall at 32 hpf, the caudal hematopoietic tissue between the DA and CV at 54 hpf, and the thymus, a definitive site of hematopoiesis, at 6 dpf ($n = 10\text{--}20$ embryos). Arrows show examples of *cmyb*⁺ cells. Yellow arrows indicate the region of the lateral trunk that is depicted in magnified images. Images captured with a 20× objective.

(B) Mean *cmyb* expression in miR-223 Δ/Δ embryos normalized to *actb1* levels and compared with wild-type as determined by qRT-PCR for three biological replicates. Bar plots show mean \pm SEM, two-tailed Student's t test.

(C) Representative micrographs (25×) of the lateral trunk in embryos expressing *Tg(kdrl:ras-mCherry)*^{s896} and *Tg(cmyb:GFP)*^{z169}. Arrows point to examples of *kdrl*⁺*cmyb*⁺ cells budding from the DA ventral wall at the peak of hematopoiesis. Yellow arrows show region of the lateral trunk that is captured in zoomed-in images.

(D) Bar plots show the average of replicate means \pm SEM of *kdrl*⁺*cmyb*⁺ cell number at 36 hpf ($n = 4$ replicates).

(E) Violin plots show *kdrl*⁺*cmyb*⁺ cell number probability density distributions. Solid lines in box plots depict median values. Phenotypic variability was not significantly different from wild-type, $p = 0.24$ by Levene's test ($n = 36$ embryos).

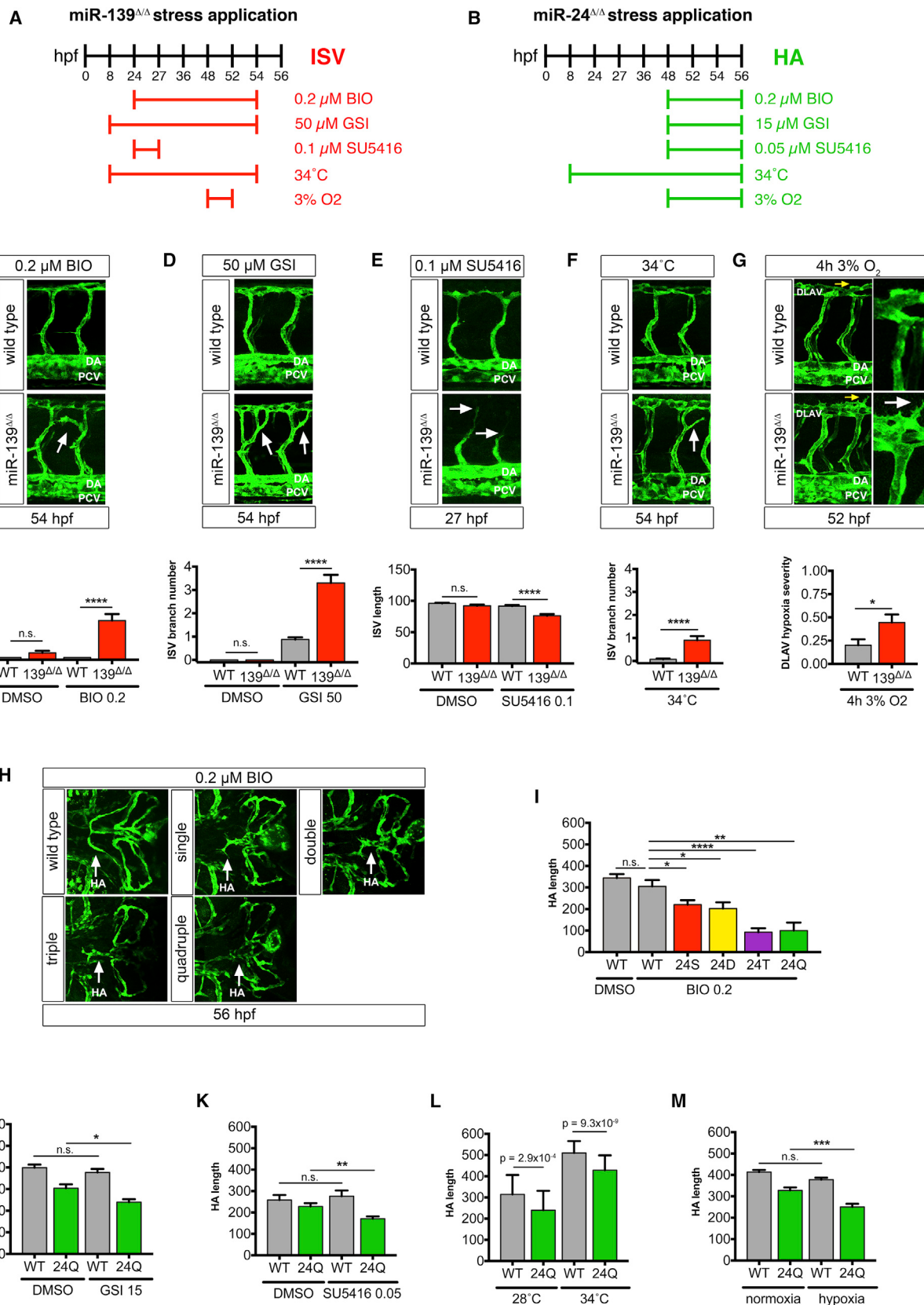
(F) Bar plots show average replicate SD \pm SEM of *kdrl*⁺*cmyb*⁺ cell number ($n = 4$ replicates).

Significance calculations were relative to wild-type embryos. n.s., not significant ($p > 0.05$); * $p \leq 0.05$, ** $p \leq 0.01$, two-tailed Mann-Whitney U test unless otherwise indicated. Abbreviations as defined in Figure 1.

variability. However, as all the endothelial miRNA mutant embryos equally survived and did not experience adverse complications, the physiological requirement of these diverse modes of miRNA function was unclear. As previously suggested in invertebrates (Cassidy et al., 2013; Ren and Ambros, 2015), we hypothesized that the aberrant phenotypic heterogeneity associated with miRNA loss might be the result of a genotype sensitized to variable perturbations. For this reason, we assessed the sensitization of miRNA-regulated traits to measurable stresses in the absence of miR-139, miR-24, and miR-223 activity.

To stress miR-139 Δ/Δ and miR-24 Δ/Δ , we used drugs targeting angiogenesis, high temperature, and hypoxic conditions at doses and exposure times that had no or little effect on wild-type embryos (Figures 6A and 6B). Treatment of miR-139 Δ/Δ with a low dose of the pro-angiogenic drugs BIO, a Wnt signaling agonist, or GSI, a Notch signaling antagonist (Gore et al., 2011; Leslie et al., 2007), resulted in increased ectopic ISV branch

number (Figures 6C and 6D). Conversely, exposure to anti-angiogenic vascular endothelial growth factor (VEGF) receptor antagonist SU5416 (Cannon et al., 2010) stunted miR-139 Δ/Δ ISV growth (Figure 6E). Strikingly, miR-139 Δ/Δ embryos were not only affected by drugs that disrupt angiogenic signaling, but were also sensitized to other forms of stress. In the absence of miR-139 activity, high temperature and hypoxia resulted in ectopic ISV branching and hypersprouting of the adjoining DLAV (dorsal longitudinal anastomotic vessel), respectively (Figures 6F and 6G) (Pype et al., 2015; van Rooijen et al., 2010). Importantly, miR-24 Δ/Δ zebrafish were also broadly sensitized to stress. All miR-24 Δ/Δ genotypes had shortened HA length upon perturbations compared with control embryos (Figures 6H–6M). The profound anomalies dictated by mild stress exposure in miR-139 Δ/Δ and miR-24 Δ/Δ allelic series supported a true phenotypic sensitization of the mutant background rather than a simple genetic interaction between the miRNA and the



(legend on next page)

stressor-induced signaling pathway. Consistent with our hypothesis, miR-223Δ/Δ embryos were not sensitized to a sub-dose of S-nitroso-N-acetyl-DL-penicillamine (SNAP), a nitric oxide donor that enhances HSPC formation at high doses (North et al., 2009) (Figures 7A–7C). The lack of drug sensitization could not be explained by a production limit in this cell type in the mutant background, as miR-223Δ/Δ embryos treated with SNAP displayed the expected enhancement of *kdrl*⁺*cmyb*⁺ cells (Figure S6).

Altogether, increased phenotypic variability associated with the loss of specific miRNAs sensitized developing traits to a broad spectrum of perturbations.

DISCUSSION

The physiology of tissues and organisms is achieved by a collection of cell behaviors possessing a spectrum of phenotypes compatible with functionality. Here, we establish that miRNA activity helps establish this optimum in the developing vertebrate embryo. Endothelial-expressed miR-139 and miR-24 influence vascular trait robustness (Figure 7D). Mutant traits were near the wild-type optimum mean value, but manifested an unexpected increase in variance. Such phenotypic behavior coincided with the ability of miRNA mutant genotypes to respond to mild stress treatments including multiple chemical drugs, high temperature, and hypoxia (Figure 7D). In contrast to miR-139 and miR-24, miR-223 only functions in HSPC trait construction (Figure 7D). Depletion of miR-223 activity led to HSPC expansion, but within an expression range similar to that of wild-type. Congruently, perturbation by a chemical stressor did not further increase HSPC formation in miR-223 Δ/Δ embryos. Differences between miRNA regulation of phenotypic robustness and construction could intrinsically stem from traits involved in cell morphogenesis versus fate determination. However, *Drosophila* miRNAs regulate trait variance in sensory organ precursor (SOP) determination and germ cell specification (Cassidy et al., 2013; Kugler et al., 2013). Therefore, the diverse control of phenotypes is likely to depend on the specific miRNA activity rather than on the nature of the developmental trait itself.

Increased heterogeneity resulting from the loss of miR-139 and miR-24 activity uniquely affects trait distribution and sensitization to stress. For example, variance of filopodia numbers in miR-139Δ/Δ endothelial cells exceeded wild-type standards in

both directions; some mutant cells had no filopodia and others possessed excessive amounts. miR-139-depleted vessels responded accordingly to an ectopic source of both pro- and anti-angiogenic environments either by branching or stalling, respectively. We speculate that miR-139Δ/Δ cells with numerous filopodia are potentially more migratory and responsive to pro-angiogenic signaling and as a consequence produce ectopic vessels. Conversely, cells with fewer filopodia are more likely to respond to anti-angiogenic signaling and induce delayed ISV migration. Interestingly, miR-139Δ/Δ ISV growth was unaffected in physiological development, despite the mild but increased mean number of filopodia. We believe this is consistent with studies in zebrafish reporting that filopodia promote ISV endothelial cell migration, but are dispensable for ISV formation (Phng et al., 2013; Wakayama et al., 2015).

While endothelial cell filopodia number spanned the entire phenotypic spectrum in miR-139Δ/Δ, stepwise depletion of miR-24 progressively increased trait heterogeneity in a single direction, producing only smaller HA vessels. miR-24Δ/Δ stress sensitivity followed this bias regardless of the stressor, such that both pro- and anti-angiogenic treatments resulted in diminished HA length. Unidirectional phenodeviants are not uncommon and likely arise from the morphological constraints of the tissue or specific signaling pathways regulating the individual trait (Cassidy et al., 2016; Felix and Barkoulas, 2015; Irmler et al., 2004; Ren and Ambros, 2015). For example, functional and well-patterned HA growth may rely on graded distributions of angiogenic signals to ensure a perfect balance of directed cell migration and polarized cell proliferation. Indeed, disruption of VEGF gradients, either with shallow or steep gradients, led to reduced spreading of the mouse retinal vascular plexus (Gerhardt et al., 2003).

At the molecular level, transcriptome analyses of miR-139Δ/Δ, miR-24Δ/Δ, or miR-223Δ/Δ vascular cells reveal direct and indirect regulation of complex genetic networks. Identified putative target genes were highly specific to each miRNA and enriched for endothelial cell migration and HSPC specification terms that correlated with the mutant phenotypes. Therefore, we likely uncovered miRNA-dependent signaling pathways functionally responsible for trait construction and/or variance.

Based on the well-established models of molecular miRNA functions (Ebert and Sharp, 2012; Herranz and Cohen, 2010), miR-139 and miR-24 could have the capacity to limit vascular

Figure 6. miR-139 and miR-24 Mutants Are Broadly Affected by Stress

(A and B) Schematic depicts the duration of chemical exposure or environmental condition used to test stress sensitivity of miR-139-regulated (A) and miR-24-regulated (B) vascular traits in the absence of miRNA activity. Stressors were administered at doses that minimally affect wild-type as indicated (see Table S1). (C and D) Arrows point to ectopic ISV branches in 54-hpf miR-139Δ/Δ embryos treated with pro-angiogenic drugs: BIO (n = 24) and GSI (n = 50–55 embryos). Controls were treated with DMSO vehicle (n = 17–24 embryos). (E) Arrows highlight stunted ISV branches in 27-hpf miR-139Δ/Δ embryos treated with anti-angiogenic VEGF inhibitor SU5416 (n = 25–27 embryos). Controls were treated with DMSO vehicle (n = 17–25 embryos). (F) Arrows show ectopic ISV branches in 54-hpf miR-139Δ/Δ embryos exposed to high-temperature stress (n = 31–44 embryos/genotype). (G) Yellow arrows show region captured in zoom images. White arrow points to hypersprouting of DLAV endothelial cells in 52 hpf miR-139Δ/Δ embryos exposed to 4 hr of hypoxia (n = 40–45 embryos/genotype). (H) Arrows indicate the HA of BIO-treated embryos. (I–M) Quantification of 56-hpf HA length (μm) upon treatment of BIO or DMSO (n = 12–24 for all genotypes except n = 6 for quadruple mutant embryos, I); GSI or DMSO (n = 15, J); SU5416 or DMSO (n = 11–16, K); high or control temperature (n = 38–50, L); and hypoxia or normoxia (n = 24, M). S = single, D = double, T = triple, Q = quadruple mutant embryos. All images were captured with a 25× objective. All bar plots represent mean ± SEM, and significance comparisons between samples are as indicated. n.s., not significant (p > 0.05); *p ≤ 0.05, **p ≤ 0.01, ***p ≤ 0.001, ****p ≤ 0.0001, two-tailed Mann-Whitney U test.

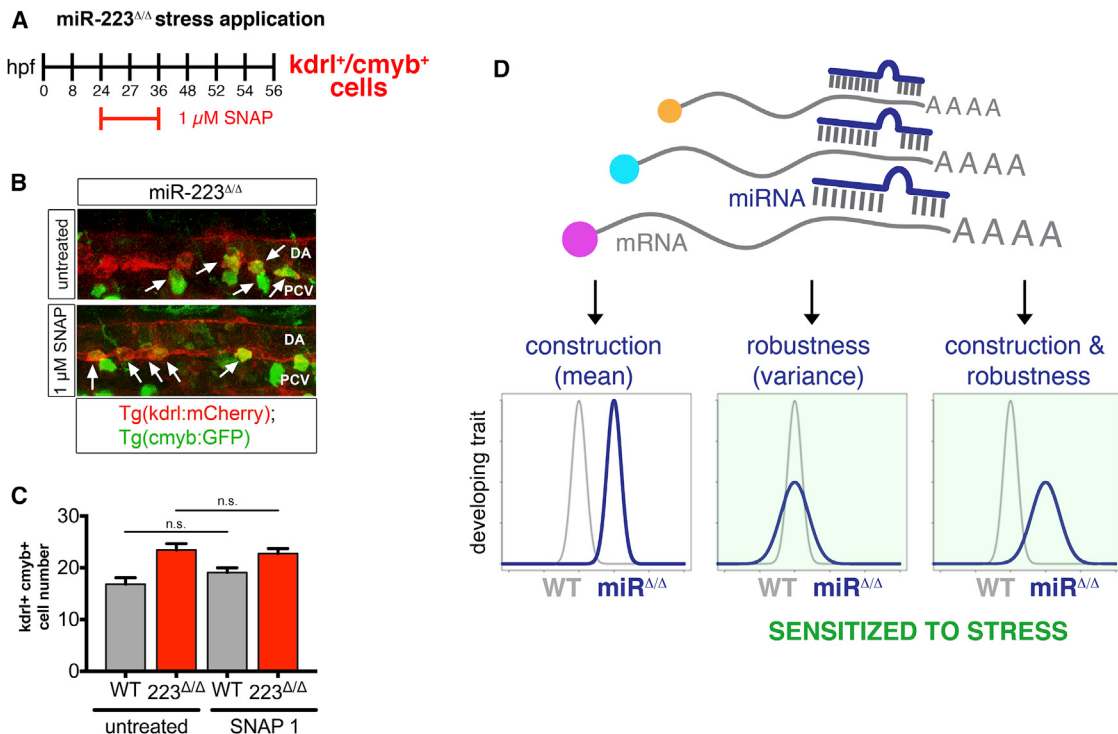


Figure 7. Phenotypic Heterogeneity Determines Trait Stress Sensitivity

(A) Schematic depicts the duration of nitric oxide donor SNAP exposure to test stress sensitivity of kdrl⁺cmyb⁺ cell number in the absence of miR-223 activity. SNAP was given at a low dose that minimally affects wild-type as indicated (see Table S1).

(B) Arrows show kdrl⁺cmyb⁺ cells budding from the DA ventral wall in untreated or SNAP-treated 36 hpf and miR-223 $^{\Delta/\Delta}$ ($n = 11\text{--}12$ embryos). 25 \times magnification.

(C) Bar plots represent mean kdrl⁺cmyb⁺ cell number \pm SEM. n.s., not significant ($p > 0.05$), two-tailed Mann-Whitney U test.

(D) Proposed model for miRNA-mediated regulation of developing traits in vertebrates. miRNA targeting of single or multiple mRNAs in complex genetic networks can control the construction and/or robustness of a phenotypic trait. Upon loss of miRNA activity, a change only in phenotypic distribution (Gaussian or otherwise) predetermines a trait's sensitivity to changing environments.

cell variance in several, but not mutually exclusive ways. First, miR-139 and miR-24 might target multiple genes that have antagonistic growth activities as observed for miR-430 (Choi et al., 2007). For example, derepression of pro- or anti-angiogenic targets in miRNA mutants could result in variable phenotypes (e.g., cells with more and fewer filopodia). The sensitivity of miRNA mutants to both pro- and anti-angiogenic signals is consistent with this example. Second, miR-139 and miR-24 could provide genetic robustness by targeting genes in feedback, feedforward, or redundant homeostatic loops, which stabilize signaling outputs upon internal and external stimuli (Ebert and Sharp, 2012; Herranz and Cohen, 2010). miRNAs are frequently positioned in such regulatory circuits, but whether genetic robustness defects result in increased phenotypic variance remains to be tested (Burke et al., 2015; Hilgers et al., 2010; Li et al., 2009; Staton et al., 2011; Verma and Cohen, 2015; Yatsenko and Shcherbata, 2014). Third, miR-139 and miR-24 may target a single gene whose precise expression defines a threshold that influences opposite vascular growth and morphogenesis phenotypes. For instance, *Drosophila* miR-9a sets a particular threshold level of its direct target, *senseless*, to determine the switch from non-SOP to SOP cell fate. Without miR-9a repression, cells stochastically adopt the SOP cell fate (Cassidy et al., 2016).

Given that more than 50 putative targets genes were regulated by miR-139 and miR-24, further investigation is required to establish which of these mechanisms regulate the variance versus construction of each trait.

Our results conceptually bridge together studies of miRNA trait variance regulation across phylogeny. With our models, we can begin to address why this developmental mechanism is highly conserved throughout the evolution of increasingly complex organisms. Notably, the miRNA gene repertoire has greatly expanded in vertebrates, with humans having the highest number of miRNA genes (Berezikov, 2011). Thus, one possibility is that miRNAs, by limiting variance, helped with the creation of more sophisticated and functional traits. Consistent with this hypothesis, factors that limit trait variance are proposed to allow cryptic genetic variation to more rapidly accumulate (Wagner, 2012). Upon loss of such factors, such as in the case of miR-139 $^{\Delta/\Delta}$ and miR-24 $^{\Delta/\Delta}$, cryptic genetic variation could become phenotypically expressed and subject to selection, thereby promoting the phenotypic evolution of a particular trait (Cassidy et al., 2016).

Stabilizing trait variability could also be a critical miRNA-mediated mechanism to prevent disease susceptibility. miRNA regulation is highly implicated in human disease, although there has

been no evidence connecting this relationship with aberrant congenital heterogeneity in phenotypes. Our data demonstrate that vertebrate miRNAs can developmentally program individuals to antagonize stress perturbation and potentially a broad range of other risk factors. Considering that the miRNAs studied here are highly conserved (Friedman et al., 2009), we speculate that this mechanism also exists in humans. SNPs in miRNA genes overlap nearly 1,000 genomic regions linked to phenotypic variations, some of which have been verified experimentally to cause the specific trait heterogeneity (Amiel et al., 2012; Huan et al., 2015). SNPs and mutations in miRNA genes and target binding sites are often associated with the probability to manifest a pathological condition such as carcinogenic transformation and cardiovascular disorders. Interestingly, the manifestation of such diseases is heterogeneous in the human population and clearly sensitive to risk factors, including genomic variation, age, and exposure to chemicals or other substances (Quiat and Olson, 2013; Ryan et al., 2010). Our results would predict that individuals lacking specific miRNA activity could inherit a set of phenotypes more prone to transformation or disease once exposed to a new environmental condition. In this respect, our discovery points to miRNA genetic variants as potential congenital markers that could help instruct the management of susceptibility factors.

Even after 20 years of miRNA biology, it is still difficult to decipher the functions of specific miRNAs, particularly in vertebrates (Lai, 2015). Only a handful of vertebrate miRNAs are necessary for major developmental decisions and for survival, while most miRNA knockouts have no phenotype unless exposed to stress or in pathological conditions (Park et al., 2012; Vidigal and Ventura, 2015). Here, we present experimental evidence that could help demystify this aspect of biology. We showed that abnormal trait variance is an early embryonic phenotype of specific vertebrate miRNA mutants and that it broadly influences their sensitivity to stress. Our data provide the groundwork for widespread mechanistic studies on how miRNAs establish an individual's genome and disease susceptibility during embryonic development.

STAR METHODS

Detailed methods are provided in the online version of this paper and include the following:

- KEY RESOURCES TABLE
- CONTACT FOR REAGENT AND RESOURCE SHARING
- EXPERIMENTAL MODEL AND SUBJECT DETAILS
 - Zebrafish Strains and Husbandry
- METHOD DETAILS
 - Generation of Zebrafish miRNA Mutants
 - Zebrafish Embryo Genotyping
 - Small RNA Sequencing Library Construction
 - mRNA Sequencing Library Construction
 - Tol2 Plasmid and Morpholino Injections
 - Northern Blot Analysis
 - Quantitative RT-PCR
 - Whole Mount *In Situ* Hybridization
 - Immunohistochemistry
 - Blood Cell Histology
 - Stress Treatments

● QUANTIFICATION AND STATISTICAL ANALYSIS

- Endothelial miRNA Classification
- Endothelial miRNA-Regulated Networks
- Quantitative RT-PCR Analysis
- Image Acquisition
- Phenotypic Trait Quantification
- Phenotypic Trait Statistical Analyses

● DATA AND SOFTWARE AVAILABILITY

SUPPLEMENTAL INFORMATION

Supplemental Information includes six figures and two tables and can be found with this article online at <http://dx.doi.org/10.1016/j.devcel.2017.02.021>.

AUTHOR CONTRIBUTIONS

D.M.K. and S.N. designed and conducted experiments, analyzed data, and wrote the manuscript. E.R. carried out experiments and analyzed data. A.M. performed the computational and statistical analyses. J.Z., D.L., M. Gu, and M. Gerstein computationally processed the raw RNA-sequencing datasets. A.G., E.F., and M.M.-M. provided materials and reagents, and C.E.V. developed the computational pipeline for the QuantSeq analysis. A.N. and G.H.-T. assembled and injected TALENs and CRISPR/Cas9. A.G., E.R., and A.M. edited the paper.

ACKNOWLEDGMENTS

The authors would like to thank Hanna Mandl for technical assistance, and Marie-Élise Schwartz and Meredith Cavanaugh for fish husbandry and care. We would also like to acknowledge Brant Weinstein for the H2B-farnesyl plasmid, and Trista North and Jenna Galloway for plasmids to make riboprobes. Finally, we are grateful to Hyung Joon Chun, Anne Eichmann, Karen Hirschi, Martin Schwartz, and Melanie Trombly for critical reading of the manuscript. This work was supported by grants from the NIH (R01HL130246 and R56HL123998 to S.N. and F32HL132475 to D.K.).

Received: June 21, 2016

Revised: January 10, 2017

Accepted: February 24, 2017

Published: March 27, 2017

REFERENCES

- Ambros, V., Lee, R.C., Lavanway, A., Williams, P.T., and Jewell, D. (2003). MicroRNAs and other tiny endogenous RNAs in *C. elegans*. *Curr. Biol.* 13, 807–818.
- Amiel, J., de Pontual, L., and Henrion-Caude, A. (2012). miRNA, development and disease. *Adv. Genet.* 80, 1–36.
- Baek, D., Villen, J., Shin, C., Camargo, F.D., Gygi, S.P., and Bartel, D.P. (2008). The impact of microRNAs on protein output. *Nature* 455, 64–71.
- Bartel, D.P. (2009). MicroRNAs: target recognition and regulatory functions. *Cell* 136, 215–233.
- Bazzini, A.A., Lee, M.T., and Giraldez, A.J. (2012). Ribosome profiling shows that miR-430 reduces translation before causing mRNA decay in zebrafish. *Science* 336, 233–237.
- Berezikov, E. (2011). Evolution of microRNA diversity and regulation in animals. *Nat. Rev. Genet.* 12, 846–860.
- Bertrand, J.Y., Chi, N.C., Santoso, B., Teng, S., Stainier, D.Y., and Traver, D. (2010). Haematopoietic stem cells derive directly from aortic endothelium during development. *Nature* 464, 108–111.
- Blevins, R., Bruno, L., Carroll, T., Elliott, J., Marcais, A., Loh, C., Hertweck, A., Krek, A., Rajewsky, N., Chen, C.Z., et al. (2015). microRNAs regulate cell-to-cell variability of endogenous target gene expression in developing mouse thymocytes. *PLoS Genet.* 11, e1005020.

- Bolger, A.M., Lohse, M., and Usadel, B. (2014). Trimmomatic: a flexible trimmer for Illumina sequence data. *Bioinformatics* 30, 2114–2120.
- Burke, S.L., Hammell, M., and Ambros, V. (2015). Robust distal tip cell pathfinding in the face of temperature stress is ensured by two conserved microRNAs in *Caenorhabditis elegans*. *Genetics* 200, 1201–1218.
- Cannon, J.E., Upton, P.D., Smith, J.C., and Morrell, N.W. (2010). Intersegmental vessel formation in zebrafish: requirement for VEGF but not BMP signalling revealed by selective and non-selective BMP antagonists. *Br. J. Pharmacol.* 161, 140–149.
- Cassidy, J.J., Jha, A.R., Posadas, D.M., Giri, R., Venken, K.J., Ji, J., Jiang, H., Bellen, H.J., White, K.P., and Carthew, R.W. (2013). miR-9a minimizes the phenotypic impact of genomic diversity by buffering a transcription factor. *Cell* 155, 1556–1567.
- Cassidy, J.J., Straughan, A.J., and Carthew, R.W. (2016). Differential masking of natural genetic variation by miR-9a in *Drosophila*. *Genetics* 202, 675–687.
- Choi, W.Y., Giraldez, A.J., and Schier, A.F. (2007). Target protectors reveal dampening and balancing of Nodal agonist and antagonist by miR-430. *Science* 318, 271–274.
- Dobin, A., Davis, C.A., Schlesinger, F., Drenkow, J., Zaleski, C., Jha, S., Batut, P., Chaisson, M., and Gingeras, T.R. (2013). STAR: ultrafast universal RNA-seq aligner. *Bioinformatics* 29, 15–21.
- Ebert, M.S., and Sharp, P.A. (2012). Roles for microRNAs in conferring robustness to biological processes. *Cell* 149, 515–524.
- Felix, M.A., and Barkoulas, M. (2015). Pervasive robustness in biological systems. *Nat. Rev. Genet.* 16, 483–496.
- Frankel, N., Davis, G.K., Vargas, D., Wang, S., Payre, F., and Stern, D.L. (2010). Phenotypic robustness conferred by apparently redundant transcriptional enhancers. *Nature* 466, 490–493.
- Friedman, R.C., Farh, K.K., Burge, C.B., and Bartel, D.P. (2009). Most mammalian mRNAs are conserved targets of microRNAs. *Genome Res.* 19, 92–105.
- Gerhardt, H., Golding, M., Fruttiger, M., Ruhrberg, C., Lundkvist, A., Abramsson, A., Jeltsch, M., Mitchell, C., Alitalo, K., Shima, D., et al. (2003). VEGF guides angiogenic sprouting utilizing endothelial tip cell filopodia. *J. Cell Biol.* 161, 1163–1177.
- Gore, A.V., Swift, M.R., Cha, Y.R., Lo, B., McKinney, M.C., Li, W., Castranova, D., Davis, A., Mukouyama, Y.S., and Weinstein, B.M. (2011). Rspo1/Wnt signaling promotes angiogenesis via Vegfc/Vegfr3. *Development* 138, 4875–4886.
- Gritz, E., and Hirschi, K.K. (2016). Specification and function of hemogenic endothelium during embryogenesis. *Cell Mol. Life Sci.* 73, 1547–1567.
- Ha, M., and Kim, V.N. (2014). Regulation of microRNA biogenesis. *Nat. Rev. Mol. Cell Biol.* 15, 509–524.
- Herranz, H., and Cohen, S.M. (2010). MicroRNAs and gene regulatory networks: managing the impact of noise in biological systems. *Genes Dev.* 24, 1339–1344.
- Hilgers, V., Bushati, N., and Cohen, S.M. (2010). *Drosophila* microRNAs 263a/b confer robustness during development by protecting nascent sense organs from apoptosis. *PLoS Biol.* 8, e1000396.
- Holmboe, K., Habicher, J., Kasza, Z., Eriksson, A.S., Filipek-Gorniak, B., Gopal, S., Couchman, J.R., Ahlberg, P.E., Wiweger, M., Spillmann, D., et al. (2012). On the roles and regulation of chondroitin sulfate and heparan sulfate in zebrafish pharyngeal cartilage morphogenesis. *J. Biol. Chem.* 287, 33905–33916.
- Huan, T., Rong, J., Liu, C., Zhang, X., Tanriverdi, K., Joehanes, R., Chen, B.H., Murabito, J.M., Yao, C., Courchesne, P., et al. (2015). Genome-wide identification of microRNA expression quantitative trait loci. *Nat. Commun.* 6, 6601.
- Irmler, I., Schmidt, K., and Starck, J.M. (2004). Developmental variability during early embryonic development of zebra fish, *Danio rerio*. *J. Exp. Zool. B Mol. Dev. Evol.* 302, 446–457.
- Isogai, S., Horiguchi, M., and Weinstein, B.M. (2001). The vascular anatomy of the developing zebrafish: an atlas of embryonic and early larval development. *Dev. Biol.* 230, 278–301.
- Isogai, S., Lawson, N.D., Torrealday, S., Horiguchi, M., and Weinstein, B.M. (2003). Angiogenic network formation in the developing vertebrate trunk. *Development* 130, 5281–5290.
- Javidan, Y., and Schilling, T.F. (2004). Development of cartilage and bone. *Methods Cell Biol.* 76, 415–436.
- Jiang, H., Lei, R., Ding, S.W., and Zhu, S. (2014). Skewer: a fast and accurate adapter trimmer for next-generation sequencing paired-end reads. *BMC Bioinformatics* 15, 182.
- Johnnidis, J.B., Harris, M.H., Wheeler, R.T., Stehling-Sun, S., Lam, M.H., Kirak, O., Brummelkamp, T.R., Fleming, M.D., and Camargo, F.D. (2008). Regulation of progenitor cell proliferation and granulocyte function by microRNA-223. *Nature* 451, 1125–1129.
- Krzywinski, M., Schein, J., Birol, I., Connors, J., Gascoyne, R., Horsman, D., Jones, S.J., and Marra, M.A. (2009). Circos: an information aesthetic for comparative genomics. *Genome Res.* 19, 1639–1645.
- Kugler, J.M., Chen, Y.W., Weng, R., and Cohen, S.M. (2013). Maternal loss of miRNAs leads to increased variance in primordial germ cell numbers in *Drosophila melanogaster*. *G3 (Bethesda)* 3, 1573–1576.
- Lai, E.C. (2015). Two decades of miRNA biology: lessons and challenges. *RNA* 21, 675–677.
- Le Guyader, D., Redd, M.J., Colucci-Guyon, E., Murayama, E., Kiss, K., Briolat, V., Mordelet, E., Zapata, A., Shinomiya, H., and Herbomel, P. (2008). Origins and unconventional behavior of neutrophils in developing zebrafish. *Blood* 111, 132–141.
- Leslie, J.D., Ariza-McNaughton, L., Bermange, A.L., McAdow, R., Johnson, S.L., and Lewis, J. (2007). Endothelial signalling by the Notch ligand Delta-like 4 restricts angiogenesis. *Development* 134, 839–844.
- Li, X., Cassidy, J.J., Reinke, C.A., Fischboeck, S., and Carthew, R.W. (2009). A microRNA imparts robustness against environmental fluctuation during development. *Cell* 137, 273–282.
- Liu, M., Yang, K.C., and Dudley, S.C., Jr. (2014). Cardiac sodium channel mutations: why so many phenotypes? *Nat. Rev. Cardiol.* 11, 607–615.
- Love, M.I., Huber, W., and Anders, S. (2014). Moderated estimation of fold change and dispersion for RNA-seq data with DESeq2. *Genome Biol.* 15, 550.
- Marusyk, A., Almendro, V., and Polyak, K. (2012). Intra-tumour heterogeneity: a looking glass for cancer? *Nat. Rev. Cancer* 12, 323–334.
- Meyen, D., Tarbashevich, K., Banisch, T.U., Wittwer, C., Reichman-Fried, M., Maugis, B., Grimaldi, C., Messerschmidt, E.M., and Raz, E. (2015). Dynamic filopodia are required for chemokine-dependent intracellular polarization during guided cell migration *in vivo*. *Elife* 4, e05279.
- Narayanan, A., Hill-Teran, G., Moro, A., Ristori, E., Kasper, D.M., A Roden, C., Lu, J., and Nicoli, S. (2016). In vivo mutagenesis of miRNA gene families using a scalable multiplexed CRISPR/Cas9 nuclease system. *Sci. Rep.* 6, 32386.
- Nicoli, S., Standley, C., Walker, P., Hurlstone, A., Fogarty, K.E., and Lawson, N.D. (2010). MicroRNA-mediated integration of haemodynamics and Vegf signalling during angiogenesis. *Nature* 464, 1196–1200.
- Nicoli, S., Knypfhausen, C.P., Zhu, L.J., Lakshmanan, A., and Lawson, N.D. (2012). miR-221 is required for endothelial tip cell behaviors during vascular development. *Dev. Cell* 22, 418–429.
- North, T.E., Goessling, W., Peeters, M., Li, P., Ceol, C., Lord, A.M., Weber, G.J., Harris, J., Cutting, C.C., Huang, P., et al. (2009). Hematopoietic stem cell development is dependent on blood flow. *Cell* 137, 736–748.
- Paffett-Lugassy, N.N., and Zon, L.I. (2005). Analysis of hematopoietic development in the zebrafish. *Methods Mol. Med.* 105, 171–198.
- Park, C.Y., Choi, Y.S., and McManus, M.T. (2010). Analysis of microRNA knockouts in mice. *Hum. Mol. Genet.* 19, R169–R175.
- Park, C.Y., Jeker, L.T., Carver-Moore, K., Oh, A., Liu, H.J., Cameron, R., Richards, H., Li, Z., Adler, D., Yoshinaga, Y., et al. (2012). A resource for the conditional ablation of microRNAs in the mouse. *Cell Rep.* 1, 385–391.
- Pham, V.N., Lawson, N.D., Mugford, J.W., Dye, L., Castranova, D., Lo, B., and Weinstein, B.M. (2007). Combinatorial function of ETS transcription factors in the developing vasculature. *Dev. Biol.* 303, 772–783.

- Phng, L.K., Stanchi, F., and Gerhardt, H. (2013). Filopodia are dispensable for endothelial tip cell guidance. *Development* 140, 4031–4040.
- Pype, C., Verbueken, E., Saad, M.A., Casteleyn, C.R., Van Ginneken, C.J., Knapen, D., and Van Cruchten, S.J. (2015). Incubation at 32.5 degrees C and above causes malformations in the zebrafish embryo. *Reprod. Toxicol.* 56, 56–63.
- Queitsch, C., Carlson, K.D., and Girirajan, S. (2012). Lessons from model organisms: phenotypic robustness and missing heritability in complex disease. *PLoS Genet.* 8, e1003041.
- Quiat, D., and Olson, E.N. (2013). MicroRNAs in cardiovascular disease: from pathogenesis to prevention and treatment. *J. Clin. Invest.* 123, 11–18.
- Raj, A., and van Oudenaarden, A. (2008). Nature, nurture, or chance: stochastic gene expression and its consequences. *Cell* 135, 216–226.
- Ren, Z., and Ambros, V.R. (2015). *Caenorhabditis elegans* microRNAs of the let-7 family act in innate immune response circuits and confer robust developmental timing against pathogen stress. *Proc. Natl. Acad. Sci. USA* 112, E2366–E2375.
- Ristori, E., and Nicoli, S. (2015). miRNAs expression profile in zebrafish developing vessels. *Methods Mol. Biol.* 1214, 129–150.
- Ristori, E., Lopez-Ramirez, M.A., Narayanan, A., Hill-Teran, G., Moro, A., Calvo, C.F., Thomas, J.L., and Nicoli, S. (2015). A dicer-miR-107 interaction regulates biogenesis of specific miRNAs crucial for neurogenesis. *Dev. Cell* 32, 546–560.
- Rutherford, S.L., and Lindquist, S. (1998). Hsp90 as a capacitor for morphological evolution. *Nature* 396, 336–342.
- Ryan, B.M., Robles, A.I., and Harris, C.C. (2010). Genetic variation in microRNA networks: the implications for cancer research. *Nat. Rev. Cancer* 10, 389–402.
- Schmiedel, J.M., Klemm, S.L., Zheng, Y., Sahay, A., Bluthgen, N., Marks, D.S., and van Oudenaarden, A. (2015). Gene expression. MicroRNA control of protein expression noise. *Science* 348, 128–132.
- Schultz, B.B. (1985). Levene's test for relative variation. *Syst. Zool.* 34, 449–456.
- Selbach, M., Schwanhausser, B., Thierfelder, N., Fang, Z., Khanin, R., and Rajewsky, N. (2008). Widespread changes in protein synthesis induced by microRNAs. *Nature* 455, 58–63.
- Staton, A.A., Knaut, H., and Giraldez, A.J. (2011). miRNA regulation of Sdf1 chemokine signaling provides genetic robustness to germ cell migration. *Nat. Genet.* 43, 204–211.
- Thisse, C., and Thisse, B. (2008). High-resolution *in situ* hybridization to whole-mount zebrafish embryos. *Nat. Protoc.* 3, 59–69.
- Ulitsky, I., Shkumatava, A., Jan, C.H., Subtelny, A.O., Koppstein, D., Bell, G.W., Sive, H., and Bartel, D.P. (2012). Extensive alternative polyadenylation during zebrafish development. *Genome Res.* 22, 2054–2066.
- van Rooijen, E., Voest, E.E., Logister, I., Bussmann, J., Korving, J., van Eeden, F.J., Giles, R.H., and Schulte-Merker, S. (2010). von Hippel-Lindau tumor suppressor mutants faithfully model pathological hypoxia-driven angiogenesis and vascular retinopathies in zebrafish. *Dis. Model. Mech.* 3, 343–353.
- Verma, P., and Cohen, S.M. (2015). miR-965 controls cell proliferation and migration during tissue morphogenesis in the *Drosophila* abdomen. *Elife* 4, e07389.
- Vidigal, J.A., and Ventura, A. (2015). The biological functions of miRNAs: lessons from *in vivo* studies. *Trends Cell Biol.* 25, 137–147.
- Vogt, G. (2015). Stochastic developmental variation, an epigenetic source of phenotypic diversity with far-reaching biological consequences. *J. Biosci.* 40, 159–204.
- Waddington, C.H. (1957). The Strategy of the Genes; a Discussion of Some Aspects of Theoretical Biology (Allen & Unwin).
- Wagner, A. (2012). The role of robustness in phenotypic adaptation and innovation. *Proc. Biol. Sci.* 279, 1249–1258.
- Wakayama, Y., Fukuhara, S., Ando, K., Matsuda, M., and Mochizuki, N. (2015). Cdc42 mediates Bmp-induced sprouting angiogenesis through Fmn13-driven assembly of endothelial filopodia in zebrafish. *Dev. Cell* 32, 109–122.
- Weiss, J.N., Karma, A., MacLellan, W.R., Deng, M., Rau, C.D., Rees, C.M., Wang, J., Wisniewski, N., Eskin, E., Horvath, S., et al. (2012). "Good enough solutions" and the genetics of complex diseases. *Circ. Res.* 111, 493–504.
- Yates, A., Akanni, W., Amode, M.R., Barrell, D., Billis, K., Carvalho-Silva, D., Cummins, C., Clapham, P., Fitzgerald, S., Gil, L., et al. (2016). Ensembl 2016. *Nucleic Acids Res.* 44, D710–D716.
- Yatsenko, A.S., and Shcherbata, H.R. (2014). *Drosophila* miR-9a targets the ECM receptor Dystroglycan to canalize myotendinous junction formation. *Dev. Cell* 28, 335–348.
- Yu, J.A., Castranova, D., Pham, V.N., and Weinstein, B.M. (2015). Single-cell analysis of endothelial morphogenesis *in vivo*. *Development* 142, 2951–2961.

STAR★METHODS

KEY RESOURCES TABLE

REAGENT or RESOURCE	SOURCE	IDENTIFIER
Antibodies		
Chicken polyclonal anti GFP	Abcam	Cat#ab13970; RRID: AB_300798
Goat anti-Chicken IgY (H+L) Secondary Antibody, Alexa Fluor 488	Thermo Fischer Scientific	Cat# A-11039; RRID: AB_2534096
Sheep Anti-Digoxigenin-AP, Fab fragments	Roche	Cat # 11093274910; RRID: AB_514497
Chemicals, Peptides, and Recombinant Proteins		
PTU (N-Phenylthiourea)	Sigma-Aldrich	Cat # P7629; CAS: 103-85-5
NBT/BCIP	Roche	Cat # 1681451
CDP Star	Roche	Cat # 12041677001
Sudan black B	Sigma-Aldrich	Cat# 199664; CAS: 4197-25-5
o-Dianisidine	Sigma-Aldrich	Cat# D9143; CAS: 119-90-4
Alcian blue	Sigma-Aldrich	Cat# A5268; CAS: 33864-99-2
BIO (2'Z,3'E-6-Bromoindirubin-3'-oxime)	Enzo Life Sciences	Cat# ALX-430-156; CAS: 667463-62-9
GSI (γ -Secretase Inhibitor IX)	Calbiochem	Cat # 565770; CAS: 208255-80-5
SU5416	Sigma Aldrich	Cat# S8442; CAS: 204005-46-9
SNAP (S-Nitroso-N-acetyl-DL-penicillamine)	Sigma Aldrich	Cat# N3398; CAS: 67776-06-1
Critical Commercial Assays		
SPLIT RNA Extraction Kit	Lexogen	Cat # 008.48
QuantSeq 3' mRNA-Seq Library Prep Kit FWD for Illumina	Lexogen	Cat # 015.24
PCR Add-on Kit for Illumina	Lexogen	Cat # 020.96
SuperScript III First-Strand Synthesis System	Invitrogen	Cat # 18080051
Kapa SYBR FAST qPCR Kit Master Mix (2X) Universal	Kapa Biosystems	Cat # KK4600
miScript II RT Kit	Qiagen	Cat # 218161
miScript SYBR Green PCR Kit	Qiagen	Cat # 218073
DIG RNA labeling kit (SP6/T7)	Roche	Cat # 11175025910
Deposited Data		
Standard RNA-seq data	this paper	GEO: GSE81341
Quant-seq data	this paper	SRA: SRP099466
Experimental Models: Organisms/Strains		
Zebrafish: AB wild-type	ZIRC	N/A
Zebrafish: miR-139 ^{ya302}	This paper	N/A
Zebrafish: miR-223 ^{ya303}	This paper	N/A
Zebrafish: miR-223 ^{ya304}	This paper	N/A
Zebrafish: miR-24-1 ^{ya324}	This paper	N/A
Zebrafish: miR-24-2 ^{ya325}	This paper	N/A
Zebrafish: miR-24-3 ^{ya326}	This paper	N/A
Zebrafish: miR-24-4 ^{ya327}	This paper	N/A
Zebrafish: <i>Tg(kdrl:gfp)</i> ^{a116}	N/A	ZDB-FISH-150901-8500
Zebrafish: <i>Tg(kdrl:ras-mCherry)</i> ^{s896} ; <i>Tg(cmyb:GFP)</i> ^{z169}	N/A	ZDB-FISH-150901-7638
Sequence-Based Reagents		
Primers for qRT-PCR and genotyping, see Table S2	This paper	N/A
Morpholino: MO-etv2 GGTTTGACAGTGCCTCAGC TCTGC	Pham et al., 2007	ZDB-MRPHLNO-070605-1

(Continued on next page)

Continued

REAGENT or RESOURCE	SOURCE	IDENTIFIER
miR-24 gRNA sequences	Narayanan et al., 2016	N/A
dre-miR-139 miRCURY LNA probe, 5'-DIG and 3'-DIG labeled	Exiqon	Cat # 35186-15
rno-miR-223 miRCURY LNA probe, 5'-DIG and 3'-DIG labeled	Exiqon	Cat # 41100-15
hsa-miR-24 miRCURY LNA probe, 5'-DIG and 3'-DIG labeled	Exiqon	Cat # 181125-15
Recombinant DNA		
Tol2-Fli1a-eGFP:pA;mCherry; 3X miR-139 MRE:pA	This paper	N/A
Tol2-Fli1a-H2B-TagBFP-p2A-EGFP-Farnesyl	Yu et al., 2015	N/A
Software and Algorithms		
Trimmomatic v0.36	Bolger et al., 2014	http://www.usadellab.org/cms/?page=trimmomatic
RNA-STAR aligners v2.4, v2.5.2a	Dobin et al., 2013	https://github.com/alexdobin/STAR
Skewer version 0.2.2	Jiang et al., 2014	https://sourceforge.net/projects/skewer/files/Binaries/
DESeq2	Love et al., 2014	https://bioc.ism.ac.jp/packages/3.1/bioc/html/DESeq2.html
TargetScan v70	Ulitsky et al., 2012	http://www.targetscan.org/fish_62/
Circos	Krzywinski et al., 2009	http://circos.ca/software/
DAVID software 6.8	NIH	https://david.ncifcrf.gov/home.jsp
Image J	NIH	https://imagej.nih.gov/ij/
Velocity Imaging Software	Perkin Elmer	N/A
Prism 7	Graphpad Software	https://www.graphpad.com/scientific-software/prism/
R Statistical Software	N/A	https://www.r-project.org/

CONTACT FOR REAGENT AND RESOURCE SHARING

Further information and requests for resources and reagents should be directed to and will be fulfilled by the Lead Contact, Stefania Nicoli (stefania.nicoli@yale.edu).

EXPERIMENTAL MODEL AND SUBJECT DETAILS**Zebrafish Strains and Husbandry**

Zebrafish were raised and maintained at 28.5°C using standard methods (unless otherwise indicated), and according to protocols approved by Yale University Institutional Animal Care and Use Committee (# 2015-11473). AB was used as the wild-type strain. Mutant strains generated in this study are miR-139^{ya302} (-9Δ), miR-223^{ya303} (-10Δ), miR-223^{ya304} (-8Δ), and miR-24-1^{ya324} (+25-2Δ); miR-24-2^{ya325} (+42-14Δ); miR-24-3^{ya326} (-9Δ); miR-24-4^{ya327} (-3Δ). The following transgenic strains were used: *Tg(kdrl:gfp)*^{la116} (ZDB-FISH-150901-8500) and *Tg(kdrl:ras-mCherry)*^{s896}; *Tg(cmyb:GFP)*^{z1169} (ZDB-FISH-150901-7638).

METHOD DETAILS**Generation of Zebrafish miRNA Mutants**

As previously described, TALENs were used to create miR-139 and miR-223 mutants and a multiplexed pool of CRISPR guide RNA pairs and Cas9 mRNA was used to simultaneously mutagenize all four miR-24 genes (Narayanan et al., 2016; Ristori et al., 2015). Both strategies were carried out in the *Tg(kdrl:gfp)*^{la116} background. Mutagenesis was initially determined by restriction endonuclease assay using CviAI (NEB) for the miR-139 locus and T7 endonuclease I (NEB) for miR-24 and miR-223 genes. Briefly, 50 ng of genomic DNA isolated with the DNeasy Blood and Tissue kit (Qiagen) from a clutch of 15-20 injected 24 hpf embryos was used to amplify a 200-400 bp region spanning the intended mutation site. Differential restriction endonuclease patterns of PCR amplicons indicated successful genome editing. Once mutagenesis was confirmed, embryos remaining in the same clutch were raised. F0 founder fish were identified and outcrossed first with AB wild-type and then with the *Tg(kdrl:gfp)*^{la116} strains to allow visualization of the developing vasculature. Mutations in adult F0 founders and subsequent generations were identified by 6-FAM fluorescent PCR fragment analysis. Genotyping PCR primers are listed in Table S2. We characterized the nature of the mutant allele by cloning the mutant PCR product in a pGEM-T Easy vector (Promega) and sequencing the resulting plasmid.

Zebrafish Embryo Genotyping

Genomic DNA from whole or portions of zebrafish embryos was extracted by boiling at 95°C for 20 minutes in 25–30 µl of 100 mM sodium hydroxide and then neutralized with ~10–12 µl of 1M Tris-HCl pH 7.5. 6-FAM fluorescent PCR was carried out with 1–3 µl of genomic DNA using genotyping primers ([Table S2](#)) and submitted for PCR fragment analysis.

Small RNA Sequencing Library Construction

To identify miRNAs enriched and/or abundantly expressed in endothelial cells, small RNA sequencing libraries were constructed as previously described ([Ristori and Nicoli, 2015](#)). Briefly, Kdrl:GFP⁺ endothelial and Kdrl:GFP⁻ non-endothelial cells were isolated by FACS from *Tg(kdrl:gfp)*^{la116} embryos at 24 hpf, 48 hpf, 72 hpf and 6 dpf stages of cardiovascular development for two biological replicates. Total RNA was extracted from both FAC-sorted populations and used to prepare small RNA libraries for deep sequencing on an Illumina platform.

mRNA Sequencing Library Construction

To identify the vascular transcripts regulated by miR-139, miR-24, and miR-223, 2–3 replicates of wild-type or miRNA mutant Kdrl:GFP⁺ endothelial cells were FAC-sorted from 27 hpf dissected trunk tissue for miR-139 and miR-223 analyses or 51 hpf dissected head tissue for miR-24 analysis. Total RNA was then isolated with the Lexogen SPLIT RNA Extraction Kit, and ~3 ng was used to prepare Lexogen QuantSeq 3' mRNA-Seq libraries for Illumina deep-sequencing according to the manufacturer's protocol. Libraries were amplified with 18 PCR cycles and any under-cycled libraries were re-amplified an additional 4–7 cycles using the Lexogen PCR Add-on Kit according to the Lexogen manufacturer's protocol.

Wild-type endothelial gene expression levels at 24, 48 and 72 hpf were determined using standard Illumina RNA-seq methods. Briefly, two replicates of Kdrl:GFP⁺ endothelial cells were FAC-sorted from 24, 48, and 72 hpf whole embryos. mRNAs were then isolated by the poly(A)-capture protocol ([Bazzini et al., 2012](#)) and used to prepare libraries for deep sequencing according to the Illumina manufacturer's protocol.

Tol2 Plasmid and Morpholino Injections

Endothelial autonomous miR-139 sensor was constructed as previously described except a synthetic 3'UTR containing 3 miRNA binding sites complementary to the mature miR-139 sequence was used instead of the *spred1* 3'UTR ([Nicoli et al., 2010](#)). Mosaic expression of the miR-139 sensor construct and tol2-Fli1a-H2B-BFP-p2A-EGFP-Farnesyl vector ([Yu et al., 2015](#)) was achieved by injecting single-cell embryos with 25 pg each of plasmid and Tol2 transposase mRNA. One-cell embryos were injected with 5 ng of *etv2* or control morpholino to prevent ISV angiogenesis ([Pham et al., 2007](#)).

Northern Blot Analysis

Total RNA from whole embryos was isolated using TRIzol reagent (Life Technologies) according to the manufacturer's protocol. 3–5 µg of total RNA was used for non-radioactive Northern blot analysis of mature miRNA levels as described before ([Nicoli et al., 2012](#)). Hybridization of dre-miR-139 miRCURY LNA probe (Exiqon) occurred at 45°C. Pixel intensity of the mature miR-139 band was quantified using Image J software and normalized to the intensity of total RNA stained with ethidium bromide. Normalized mean miR-139 levels represent three biological replicates.

Quantitative RT-PCR

Total RNA from adult fin clips or pooled embryo heads, tails, or whole bodies was isolated using TRIzol reagent (Life Technologies) according to the manufacturer's protocol. 0.5–1 µg of total RNA was used to synthesize cDNA with the miScript II RT kit (Qiagen) according to the manufacturer's protocol. miScript SYBR Green PCR kit (Qiagen) was performed as described by the manufacturer using 1 µl of cDNA. A similar procedure was followed to measure mRNA levels, except SuperScript III Reverse Transcriptase (Life Technologies) and KAPA SYBR FAST qPCR kit (Kapa Biosystems) were used instead. All qPCR reactions were carried out in triplicate for 2–5 biological replicates in CFX96 Real-Time System thermal cycler (Bio-Rad). qRT-PCR primers are listed in [Table S2](#). miRNA universal reverse primer and U6 primers (RNU6B, Hs_RNU6-2_1) were commercially provided from Qiagen.

Whole Mount *In Situ* Hybridization

Embryos subjected to whole mount *In Situ* hybridization (WISH) were raised in 0.003% PTU starting after the gastrulation stage to prevent pigmentation. Zebrafish embryos were fixed with 4% formaldehyde and WISH was performed as previously described with the following modifications ([Thisse and Thisse, 2008](#)). To detect mRNA expression, digoxigenin labeled riboprobes were synthesized using a DIG RNA labeling kit (SP6/T7; Roche Applied Bioscience) and hybridized with embryos overnight at 60°C. To detect miRNA expression, double-digoxigenin labeled miRCURY LNA probe oligonucleotides (Exiqon) were hybridized overnight at 45–55°C. Post hybridization washes occurred at the hybridization temperature and consisted of 2 × 30 minutes (min.) 2x SSCTw/50% formamide washes, 1 × 30 min. 2x SSCTw wash, and 2 × 30 min. 0.2x SSCTw. After blocking in 5% sheep serum/PBSTw for at least 1 hour, embryos were incubated overnight at 4°C in 1:10,000 sheep anti-DIG AP Fab fragments (Roche) in blocking solution. The WISH signal was revealed with 1:50 dilution of NBT/BCIP (Roche) in alkaline phosphatase buffer. When immunohistochemistry was performed with WISH, 1:300 chicken anti-GFP (AbCam) primary antibody was incubated with anti-DIG AP and 1:400 Alexa Fluor 488 goat anti-chicken IgG (ThermoFisher) secondary antibody was applied as the last step after WISH development.

Immunohistochemistry

To better visualize kdrl+ cmyb+ cells, immunohistochemistry was performed to amplify the cmyb:GFP signal as follows. After overnight 4% formaldehyde fixation at 4C, embryos were washed 4-5x with PBSTw, and then washed 3-4 x 5 min. plus 2 hours in blocking solution (0.8% Triton-X, 10% normal goat serum, 1% BSA, 0.01% sodium azide in PBSTw. Antibody concentrations used were 1:300 chicken anti-GFP (AbCam) primary antibody and 1:400 Alexa Fluor 488 goat anti-chicken IgG (ThermoFisher) secondary antibody. Following overnight antibody incubation at 4C, six washes for a total of 6 hours were performed with blocking solution lacking goat serum at room temperature.

Blood Cell Histology

Sudan black staining (Sigma-Aldrich) of neutrophils (Le Guyader et al., 2008) and o-dianisidine staining (Sigma-Aldrich) of erythrocytes (Paffett-Lugassy and Zon, 2005) was performed on at least 30 embryos per genotype from at least 3 separate clutches as previously reported. Alcian blue staining (Sigma-Aldrich) of cartilage (Javidan and Schilling, 2004) was performed on 2-3 independent clutches of at least 6 embryos per genotype except for quadruple mutants where 2 animals were examined.

Stress Treatments

Chemical or environmental stressors that interfere with the specific miRNA-regulated trait were applied at doses and exposure times that have no or minor effects on wild-type embryos as outlined in Figures 6A, 6B, and 7A, and Table S1. All stress treatments were administered in egg water with 0.003% 1-phenyl-2-thiourea (PTU) to prevent pigmentation for downstream analyses, and stopped at the indicated time points by fixing embryos with 4% formaldehyde. Drugs that disrupt angiogenic signaling included (2'Z,3'E)-6-Bromoino-dirubin-3'-oxime (BIO, Enzo Life Sciences), gamma secretase inhibitor IX (GSI, Calbiochem), and Sugen 5416 (SU5416, Sigma-Aldrich). S-Nitroso-N-acetyl-DL-penicillamine (Sigma-Aldrich) was applied to disrupt HSPC formation. PTU egg water was changed daily for high temperature experiments. For hypoxia experiments, PTU egg water was first pre-depleted of oxygen in a hypoxic chamber, gassed with 3% oxygen/5% carbon dioxide/nitrogen mixture (AirGas) for 10 minutes at 2 PSI and sealed overnight. The next day, embryos in petri dishes were exposed to hypoxia by replacing the PTU egg water with the oxygen-depleted water and placing them in a hypoxic chamber, gassed as described above and sealed for the duration of the experiment. All stress treatments were carried out at least 2-3 times.

QUANTIFICATION AND STATISTICAL ANALYSIS

Endothelial miRNA Classification

Small RNA-seq reads were trimmed of Illumina adaptor sequences using Trimmomatic v 0.36, (Bolger et al., 2014) and resulting reads were mapped to the zebrafish Zv9 zebrafish genome version using RNA-STAR aligners v.2.4 (Dobin et al., 2013). Uniquely mapped small RNA-seq reads were counted at each gene locus, and normalized to total reads per million (RPM). We identified the most abundant and/or enriched miRNAs in endothelial cells, which we termed “endothelial miRNAs”. Abundant miRNAs were within the third quartile of the expression distribution for each stage of development in endothelial cells. Endothelial-enriched miRNAs had a greater than two fold average change in gene expression in endothelial compared to non-endothelial cells.

Endothelial miRNA-Regulated Networks

Reads from QuantSeq mRNA libraries were trimmed of the adapter (AAAAAAAAAAAAAAAGATCGGAAGAGCA-CACGTCTGAACCT CAGTCAC) using Skewer version 0.2.2 with default parameters (Jiang et al., 2014) and mapped to the zebrafish genome Zv9 using RNA-STAR aligners v2.5.2a (Dobin et al., 2013) with the following non-default parameters: `-alignEndsType Local -seedSearchStartLmaxOverLread 0.8 -sjdbScore 2`. Genomic sequence indices for RNA-STAR were built including exon-junction coordinates from Ensembl r78 (Yates et al., 2016). Read counts per gene were computed by summing the total number of reads overlapping with a minimum of 10 nucleotides of the annotation including only uniquely mapped reads in the genome. Per gene annotation was obtained by concatenating all Ensembl isoforms together. To determine significantly over- and under-expressed genes between WT and miRNA mutant conditions, gene read counts were compared using DESeq2 (Love et al., 2014). Genes below 5 counts in all replicates in either condition were excluded from the analysis. Differentially expressed genes in each data set were then examined for miR-139, miR-24, or miR-223 binding sites using TargetScan v70 (Ulitsky et al., 2012).

Reads from standard RNA-seq libraries were trimmed of Illumina adaptor sequences using Trimmomatic v 0.36, (Bolger et al., 2014) and resulting reads were mapped to the zebrafish Zv9 zebrafish genome version using RNA-STAR aligners v2.5.2a (Dobin et al., 2013). Uniquely mapped reads were counted as described above for Quant-seq analyses.

The Circos software package (Krzywinski et al., 2009) was used to provide a genome-wide view of the identified miRNA-regulated genes and their stage-specific expression level in endothelial cells. Using the DAVID software, Gene Ontology terms were assigned to miRNA target genes that were upregulated in the corresponding miRNA mutant.

Quantitative RT-PCR Analysis

The $2^{-\Delta CT}$ or the $2^{-\Delta\Delta CT}$ methods were used to determine relative gene expression for quantitative RT-PCR analyses. Mature miRNA expression was normalized to U6 snRNA levels and relative to wild-type. mRNA levels were normalized to the beta actin housekeeping gene, *actb1*. Statistical comparisons between wild-type and mutant were determined by an unpaired, two-tailed Student's t-test.

Image Acquisition

The majority of fluorescent images were captured using a Leica Microsystems SP5 confocal microscope using a 25X objective except for images of ISVs in [Figures 3](#) and [6](#) that were taken with a 40X objective. Max projections were generated with the Leica application suite or Perkin Elmer Velocity software. All differential interference contrast microscopy images and fluorescent images in [Figures 1E](#) and [1F](#) were acquired with the Nikon Eclipse 80i microscope with a 20X objective.

Phenotypic Trait Quantification

Quantified traits were selected based on a change in phenotypic expression between wild and mutant sample populations. Trait measurements were performed on confocal max projections or bright field images. All length measurements were obtained using Image J. ISV length was measured from the DA to the end of the growing vessel. HA size was determined by the sum of several measurements along the entire vessel length including both branches that bifurcate from the central stem. The severity of DLAV hypersprouting in response to hypoxia was based on the following scale: 0 = no, 1 = partial, 2 = full hypersprouting along the length of the DLAV. All values are presented with mean \pm SEM unless otherwise indicated, and the number (n) of samples analyzed is indicated in figure legends.

Phenotypic Trait Statistical Analyses

Statistical analyses on trait measurements under physiological conditions are as follows ([Figures 3, 4, and 5](#)). Filopodia number was counted for 4 ISV endothelial cells in 9 replicate embryos (except for one mutant replicate which had 5 cells). HA length was measured for 4 replicates of 10 embryos (except for one quadruple mutant replicate which had 8 embryos). *kdr1⁺ cmyb⁺* cells were counted for 6 replicates of 6 embryos. Replicate means and standard deviations were averaged for each genotype. Due to the low replicate number, a non-parametric Mann-Whitney U-test was applied to test for statistical differences between wild-type and mutant phenotypes. After first confirming similar variances between genotype replicates with Levene's Test for equality of variances, measurements within a genotype were pooled into a single dataset (i.e. n = 36-40) in order to test for trait variability differences between wild-type and mutant embryos. Each pooled dataset is depicted with a violin plot showing its probability density distribution, and was tested for normality using the Shapiro-Wilk test. Not all genotypes were normally distributed, so the more stringent non-parametric Levene's Test was applied with a cutoff p-value ≤ 0.05 to discard the null hypothesis ([Felix and Barkoulas, 2015; Schultz, 1985](#)). For stress sensitivity experiments ([Figures 6 and 7](#)), measurements from 2-5 replicates per treatment were combined and a Mann-Whitney U-test applied to detect statistical differences between conditions. Importantly, replicates within a genotype were not statistically different from each other (Mann-Whitney U-test). All statistical tests were performed using R or Graphpad Prism, and the car R package was used for Levene's test. p-values ≤ 0.05 were considered statistically significant.

DATA AND SOFTWARE AVAILABILITY

Standard RNA-seq experiments are submitted to the Gene Expression Omnibus (<http://www.ncbi.nlm.nih.gov/geo/>) under accession number GEO: GSE81341. Raw Quant-seq reads are publicly accessible in the Sequence Read Archive under SRP099466.